Transcriptional profiling of skin cancer NK cells reveals the elevated glucocorticoid signaling switches their anti-tumor characteristics to a homeostatic feature

Qin Wei[1,2], Guirong Liang[1,2], Yuancheng Li[1], Rui zeng[1], Anlan Hong[1], Hongsheng Wang[1], Suying Feng[1], Yan Wang[1*], Yetao Wang[1,3*]

1 Hospital for Skin Diseases, Institute of Dermatology, Chinese Academy of Medical Sciences and Peking Union Medical College, Nanjing, China
2 These authors contributed equally
3 Lead Contact
*Correspondence: drwangyan@163.com; yetaowang@163.com

Summary

The interplay between natural killer (NK) cells and tumor microenvironment (TME) is closely associated with tumor progression. We showed NK cells are common constituents in the tissue of skin cancers including basal cell carcinoma (BCC), cutaneous squamous cell carcinoma (cSCC), extramammary paget disease (EMPD) and acral melanoma (aMM). scRNA-Seq revealed an inter and intra-tumor transcriptional heterogeneity of NK cells dependent on different skin TMEs. Unexpectedly, compared to peri-tumor, skin tumor NK cells down regulated the production of anti-tumor cytokines, IFN-γ and TNF-α, and up regulated the production of amphiregulin (AREG), a ligand of epidermal growth factor receptor (EGFR), which functions in promoting skin tumor growth and mediating immune tolerance. Mechanistically, skin TME upregulated NK cell glucocorticoid receptor (GR, NR3C1) activity, which specifically induced NK cell AREG production, and switched the anti-tumor characteristics of NK cells to a homeostatic feature. NR3C1 knockout or GR inhibitor abolished NK cell AREG production. Finally, we showed primary GR activation induced a memory response of AREG production by NK cells upon secondary stimuli, however pro-inflammatory cytokine induced memory response of IFN-γ production was inhibited by GR activation. These findings highlight the glucocorticoid receptor-NK cell-AREG axis may serve as a potential target for anti-cancer therapies.

Keywords

NK cells, AREG, Glucocorticoid receptor, Skin cancer, Tumor microenvironment

Introduction

Skin cancers are the most common human malignancies, including melanoma (MM) and non-melanoma skin cancers (NMSCs), the latter account for >90% of all skin cancers[1–3], mainly comprises basal cell carcinoma (BCC), cutaneous squamous cell carcinoma (cSCC) and extramammary paget disease (EMPD)[2,3]. Although surgery remains effective treatment, immune therapies targeting PD-1 and CTLA-4 have shown promising clinical results in unresectable or metastatic/advanced BCC, cSCC and MM[3–6]. Tumor microenvironment (TME) plays critical roles in responsiveness of checkpoint therapies. Unfavorable TMEs result in resistance of treatment and poor prognosis[5,7], underlining the requirement of defining determinants of unresponsive TME and associated biomarkers.

As innate counterpart of cytotoxicity T cells, natural killer (NK) cells play pivotal roles in restricting tumor growth and metastasis by releasing perforin and granzymes containing lysosomes, by engaging death receptors and by producing pro-inflammatory cytokines such as IFN-γ and TNF-α[8]. Adoptive transfer of NK cells is not restricted by human leukocyte antigen (HLA) and do not cause graft-versus-host disease (GvHD), multiple sources such as $CD34^+$cell, iPSCs, peripheral blood mononuclear cells (PBMCs) and cord blood have been used for clinical preparation of therapeutic NK cells. These advantages render NK cells becoming the focus of anti-tumor research[8,9]. Moreover, NK cells play important roles in determining effectiveness of checkpoint therapies by modulating TME, for example, NK cells positively regulate the abundance of intratumoral stimulatory dendritic cells by producing FLT3LG, and determine the responsiveness of anti-PD-1 therapy against melanoma[7], and dysfunctional NK cell infiltration is associated with progression of cSCC[10]. The detailed characterization of skin cancer NK cells and their crosstalk with TME should provide important information for immune therapy of skin cancers.

Amphiregulin (AREG) is a ligand of epidermal growth factor receptor (EGFR), which plays important roles in promoting tumor growth and metastasis by enhancing cell survival, proliferation, angiogenesis and mediating immune tolerance[11–14]. The enhanced production of AREG in TME also contributes to therapeutic resistance, therefore, AREG becomes a promising target of cancer therapies[13,15–17]. Our recent study showed that unlike mouse NK cells, the chromatin region around AREG promoter is only open in human NK cells and $AREG^+$NK cells play a homeostatic function in HIV-1 induced inflammation[18]. However, the physiological stimulus for NK cell AREG production and their crosstalk with TME is not clear.

Here, we thoroughly investigated the transcriptome and biological function of NK cells in the paired peri-tumor and tumor tissues from BCC, cSCC, EMPD and acral

melanoma (aMM), and revealed the heterogeneity of NK cells in different TMEs. Skin tumor NK cells exhibited enhanced production of AREG due to the elevated glucocorticoid receptor (GR) activity in TME. GR activation suppressed anti-tumor characteristics and promoted homeostatic features of NK cells. We also showed NK cells exhibited a memory-like response to the GR activation. These researches reveal an unexpected effect of skin TME on the anti-tumor function of NK cells.

Results

NK cells are stable constituents of skin tumor lymphocytes

To investigate the common and the unique features of NK cells in different skin cancers, fresh isolated, site and donor matched tumor and normal peri-tumor tissue from BCC, cSCC, EMPD and aMM were processed for single cell transcriptome and function analysis (Figure 1A and STAR Methods), 24 and 68 paired samples were collected for single cell RNA-Seq (scRNA-Seq) and flow cytometry detection respectively (Figures 1A, S1 and Table S1).

To avoid large proportions of skin epithelial cells and fibroblasts that limit in depth characterization of NK cells[6,19], $CD45^+$ cells were enriched before library preparation (STAR Methods). 217,037 cells were identified by Cell Ranger with an average depth of 49,004 mean reads/cell, 146,643 $CD45^+$ cells were identified after filtering by Seurat and removal of non-hematopoietic cells (Table S2 and STAR Methods). Skin $CD45^+$ cells formed 8 clusters which represented NK cell, T cells, B cells, plasma blasts, dendritic cells, monophagocytes, mast cells and neutrophils in uniform manifold approximation and projection (UMAP) (Figure 1B and 1C). The identity of 2282 high quality NK cells were confirmed by their specific expression of NK cell markers (NKG7, GZMB, GNLY, KLRD1, IFNG) and no expression of markers for other cell types (Figures 1C,1D and S2A)[18,20,21].

Flow cytometry was performed to confirm the result of scRNA-Seq. 14 lineage antibodies (against CD3, CD4, TCRαβ, TCRγδ, CD19, CD20, CD22, CD34, FcεRIα, CD11c, CD303, CD123,CD1a, and CD14) were used to exclude T cells, B cells, monocytes/macrophages, dendritic cells and other lineage positive cells from CD45 positive population, NK cells were defined as Lin^-TBX21^+ cells according to previous studies by others and us (Figure 1E)[18,20,22]. The result showed NK cells represent a significant lineage negative population in both tumor and peri-tumor tissues from four types of skin cancer (Figure 1E). Although the percentage of NK cells between tumor and peri-tumor tissue were not altered (Figure 1F), the numbers of NK cells were

increased in tumor tissue (Figure 1G), consistent with the increased percentage and numbers of $CD45^+$ cells in the tumor (Figure 1H and 1I).

Transcriptional heterogeneity of NK cells in different skin TME

Total skin NK cells were reclustered into 5 populations, no significant bias of distribution was observed due to donors or skin tumor types (Figures 2A, 2B, S2B and Table S3), indicating the clustering was predominantly driven by the transcriptional profile of NK cell clusters rather than tumor types or batch effect. Cluster 0 (C0) NK cells highly expressed IL2RA, IL7R, TCF7 and BACH2, markers of blood $CD56^{hi}$NK cells reported by others and our previous studies[18,20,23]; C1 NK cells highly expressed HAVCR2, FCGR3A, PRF1 and CST7, markers of blood $CD56^{dim}$NK cells[18,20]; C2 NK cells exhibited the highest expression of EGFR ligand AREG, tissue infiltrating markers RGS1 and CD69[24], and AP-1 family members (JUN, ATF3 and FOSB); C3 NK cells highly expressed inflammatory cytokine encoding genes TNF and IFNG; C4 NK cells highly expressed tissue resident marker CXCR6[24], and GZMA, HLA-DRA, TIGIT and TNFRSF9; Consistent with previous study[25], C5 NK cells that highly expressed interferon stimulated genes (IFIT1, IFIT3, MX2, ISG15, ISG20), represented a minor NK cell population in the skin (consist only 25 cells), were not focused for further analysis (Figure 2C and Table S3).

Differentially expressed genes (DEgenes) of each NK cell cluster between tumor and peri-tumor tissue from 4 types of skin cancer were analyzed using Seurat FindAllMarkers ($P<0.05$, $Log_2FC>0.36$) (Table S4). Signature DEgenes associated with NK cell activation[8], type I interferon response[26] and tumor stress[27,28] (Table S5) that are critical for NK cell anti-tumor activity were extracted for gene set score analysis. Compared to peri-tumor, only tumor NK cell clusters from cSCC and aMM (except C3) exhibited elevated NK cell activation signature (Figure 2D). Similar pattern was also observed for type I interferon response signature with an exception of C0 from BCC and C3 from cSCC (Figure 2E). The elevated tumor stress signature was observed in different NK cell clusters from BCC, cSCC, EMPD and aMM (Figure 2F). These results revealed an inter and intra-tumor heterogeneity of NK cells in response to different skin TMEs.

The transcriptional regulatory networks (regulons) in each skin cancer were identified using SCENIC (Figure 3A and Table S6)[29]. The altered activity of regulons (DEregulons) between peri-tumor and tumor NK cells were calculated based on their average AUCell scores in each NK cell cluster ($P<0.05$, $Log_2FC>0.5$). The DEregulons and the numbers of their regulated DEgenes were shown in Figure 3A. In BCC, the activity of IKZF2 that inhibits NK cell IFN-γ production and degranulation was upregulated, and the activity of

AP-1 members (FOSB and JUNB) that required for NK cell cytotoxicity were downregulate in tumor NK cells[30,31]; In cSCC, BACH1 activity which suppresses the transcription of anti-inflammatory factor HO-1[32], was downregulated in tumor NK cells. In EMPD, the activity of HDAC1 that is important for the expression of NK cell activating receptor NKG2D, was downregulated in tumor NK cells[33]. In aMM, the activity of AP-1 member JUN was upregulated, and the activity of HIF1A that directs NK cell metabolic adaptation to TME and suppresses their anti-tumor function, was downregulated in tumor NK cells[34];

Unique characteristics for each NK cell cluster in skin cancers

To characterize the unique impact of different TMEs on NK cell clusters, the unique DEgenes belonging to each NK cell cluster (not shared by other clusters) in the tumor of BCC, cSCC, EMPD or aMM were analyzed compared to their counterparts in the peri-tumor (Figures 3B-3E, S3A and Table S7).

In BCC (Figure 3B and Table S7), cluster unique genes that sense or respond to stress were upregulated in C0 (GADD45A)[35], C1 (DNAJB1, HSPE1, MTCH1), C2 (DNAJC7, EGR1, TXNIP)[36,37] and C4 (DUSP1)[38], and were downregulated in C2 (HSPA8), C3 (GADD45B) and C4 (HSP90B1). Genes that potentiate NK cell infiltration, effector function and fitness upon activation were upregulated in C0 (PIK3C2A, CCL4, JAK1, KLF6, KDM6A, TAX1BP1, SLC4A7)[39–43], C1 (SLC7A5, CD44, TNFSF14)[44,45], C2 (EOMES, ZBTB1, IKZF1, DOCK8)[46–48], C3 (GZMK) and C4 (ID2)[49], and were downregulated in C0 (GNLY, CTSW)[50], C1 (LYST, SH2D1A, IRF3, OASL)[51], C2 (GZMB, SAT1)[52], C3 (CD226, CEBPG)[53,54] and C4 (PRF1, FCGR3A, RUNX1)[55]. This paradoxical expression pattern of stress and NK cell activation associated genes was consistent with the unchanged tumor stress (C2-C4) and NK cell activation (C0-C4) signatures between tumor and peri-tumor in BCC (Figures 2D and 2F).

The dysregulated signatures of stress and NK cell function were also observed in EMPD and aMM (Figures 3D, 3E and Table S7). For example, NK cell activating receptor KLRC2 and its adaptor TYROBP were uniquely upregulated in C0 and C2[56,57], whereas the GZMK and the cytotoxic trigger CD44 were downregulated in the same clusters in EMPD. (Figure 3D)[58]. XBP1 and STAT3, which potentiate NK cell tumor killing activity were uniquely up and down regulated in C0 in aMM[59,60]. The bi-directional change of genes required for NK cell effector function indicated a disturbed anti-tumor activity of NK cells in BCC, EMPD and aMM.

In cSCC (Figure 3C and Table S7), a relatively consistent trend for an upregulation of cluster unique genes that enhancing NK cell activation or expansion were detected in

C0 (CD2, CD52)[61,62], C1 (NCR3, OASL, NFKBIZ, TSC22D4)[63,64], C2 (KLRC3, IKZF3, ETS1, NFIL3, JAK1, NKTR)[65,66], and C4 (GNLY, TNFSF10)[67], and a downregulation of immunosuppressive genes were concertedly detected in C0 (USP14)[68], C1 (TNFRSF18, HLA-B, HLA-C)[69–71], and C4 (IKZF2, LAG3, KIR2DL1)[30], consistent with the elevated NK cell activation signatures in all NK cell clusters from the tumor of SCC. (Figure 2D).

Interestingly, C0 or C2 NK cells in BCC, SCC and EMPD uniquely upregulated glucocorticoid receptor NR3C1 (GR) (Figures 3B-3D and Table S7), a major target of anti-inflammation and anti-cancer therapies[72,73], suggesting C0 and C2 NK cells may play a role in inducing immune tolerance TME.

Skin TME enhances NK cell AREG production

Expect for producing tumor restrictive cytokines IFN-γ and TNF-α, we recently showed, unlike mouse NK cells, human blood NK cell can express EGFR ligand AREG[18], which play important roles in stimulating proliferation of keratinocytes and fibroblasts[74,75], promoting tumor growth and metastasis[11–14], and inducing immune tolerance and therapeutic resistance in anti-cancer treatment[13,15–17]. However, the production of AREG by skin NK cells and their crosstalk with skin TME have not been investigated.

Our single cell transcriptome analysis showed AREG was mainly expressed by C0 and C2 skin NK cells, whereas, IFNG and TNF were mainly expressed by C2 and C3 NK cells (Figures 2C and 4A). In line with the expression profile, the protein of AREG, IFN-γ and TNF-α were readily detectable from tumor and peri-tumor NK cells in BCC, cSCC, EMPD and aMM by flow cytometry (Figure S3B). Compared to peri-tumor, tumor NK cells exhibited an elevated production of AREG in BCC and cSCC, a similar trend was also observed in EMPD and aMM (Figure S3B), however, tumor NK cells exhibited a decreased production of IFN-γ and TNF-α in BCC, and a decreased TNF-α production in cSCC (Figure S3B). In pan skin cancer analysis, skin tumor NK cells commonly exhibited an upregulated AREG and downregulated TNF-α production (Figure 4B-4D), though IFN-γ production did not change (Figure 4E)

Based on the contrasting biological function between AREG and IFN-γ or TNF-α in tumor progression, NK cells were further divided by their ability to produce these cytokines. The percentage of both $AREG^{+}IFN\text{-}\gamma^{-}$ and $AREG^{+}IFN\text{-}\gamma^{+}$ NK cells was increased, whereas the percentage of $AREG^{-}IFN\text{-}\gamma^{+}$NK cells was decreased in the skin tumor tissue (Figures 4F-4I); Similarly, the skin TME affected the percentage of $AREG^{+}TNF\text{-}\alpha^{-}$ and $AREG^{-}TNF\text{-}\alpha^{+}$NK cells oppositely, though the percentage of $AREG^{+}TNF\text{-}\alpha^{+}$ NK cell was not changed (Figures 4F and 4J-4L). The percentage of

AREG$^+$NK cell subsets (including AREG$^+$IFN-γ$^-$ and AREG$^+$IFN-γ$^+$) inversely correlated with NK cells that are single positive for IFN-γ (Figures 4M and 4N), however, the AREG$^+$ and TNF-α$^+$ NK cell subsets were not significantly correlated (Figures 4O and 4P). These results revealed an altered production of pro- and anti-tumor cytokines by NK cells in skin TME.

Glucocorticoid receptor activation specifically induces NK cell AREG production

To understand how skin TME affects NK cell AREG production, we tested 14 stimuli that are important for NK cell proinflammatory cytokines production, cytotoxicity, and expansion, including NK cell activating cytokines, receptor ligands, antibodies and their combinations, none of these conditions induced NK cell AREG production (Figure S4A). However, when comparing the DEgenes between AREG$^+$NK cells (C0, 2) and AREG$^-$NK cells (C1, 3, 4, 5) (Figures 4A and 5A), we found the expression of glucocorticoid target genes were uniformly higher in AREG$^+$NK cells than in AREG$^-$NK cells (Figure 5B)[76–79]. The gene set score analysis also showed AREG$^+$NK cells exhibited higher glucocorticoid receptor (GR) activity scores than AREG$^-$NK cells (Figure 5C and Table S5)[76–79]. Moreover, the score of GR activity but not NK cell activation positively correlated with the score of tumor stress (Figures 5D, 5E and Table S5). Compared to peri-tumor, the expression of AREG was co-upregulated with GR target genes in the skin tumor C0 and C2 NK cells (Figure 5F), consistent with the upregulated glucocorticoid receptor (NR3C1) in these NK cell clusters in the skin tumor (Figures 3B-3D). These evidence suggested that the upregulated GR activity in skin TME is responsible for the elevated AREG production by NK cells.

To validate the above hypothesis, PBMCs were treated with dexamethasone (Dex), a synthetic glucocorticoid that was widely used in anti-inflammation therapies. The result clearly showed that Dex robustly induced the AREG production by NK cells but not by other cell types in the PBMCs (Figures 5G and 5H). Similar results were achieved by using other versions of glucocorticoids such as betamethasone and methylprednisolone (Figures S4B and S4C).

One NR3C1 binding site was detected in the open chromatin region around AREG promoter in NK cells by JASPAR motif analysis (http://jaspar.genereg.net/) (Figure 5I). Cas9/RNP mediated NR3C1 knockout was performed in NK cells, the result showed that NR3C1 knockout suppressed the Dex induced AREG production to AREG knockout level (Figure 5J and Figure S4D). Finally, we showed Dex inhibitor Mifepristone (also known as RU486) strongly inhibited Dex induced AREG production by NK cells (Figures 5K and 5L). These results demonstrated that the elevated GR activity in the skin tumor NK cells led to their enhanced AREG production.

GR activation induces a homeostatic program of NK cells

To systematically investigate the effect of GR activation on NK cells, we performed bulk RNA seq on NK cells in steady state or upon cytokine stimulation in the presence or absence of dexamethasone (Dex). First, CD56^{dim}NK cells were sorted from untreated and Dex-treated PBMCs, then were subjected to bulk RNA-Seq (Figure S5A). AREG exhibited the highest fold change in 102 Dex upregulated genes which enriched in response to steroid hormone (FKBP5, KLF9, CFLAR, TSC22D3)[77–79], and negative regulation of NK and T cell activation, cell proliferation, programmed cell death and apoptotic process (CFLAR, PRDM1, TSC22D3, TLE1, TNFAIP8, PIK3IP1, TXNIP, HPGD, PTGER2, ZFP36L2, CD55, FOXO1)[78,80–88](Figures 6A, 6B and Table S8). Many of these genes have been reported as GR targets and contributed to resistance of anti-tumor therapy, for example, PRDM1 decreases the sensitivity of NK cells in response to IL-2 and inhibits their IFN-γ and TNF-α production[89–91]; TSC22D3 comprises anti-tumor therapy by blocking type I interferon response of DCs and activation of IFN-γ^{+}T cells[78]; TLE1 negatively regulates NF-kB and WNT signaling that controls NK cell effector function and pro-inflammatory memory response[20,82,83,92]; HPGD, PTGER2 and ZFP36L2 are important for maintaining tissue homeostasis by suppressing NK or T cell induced inflammation (Figure 6A and Table S8)[85,86,93,94].

On the contrary, upon Dex treatment, genes involved in response to type I and II interferon, positive regulation of TNF production, programmed cell death and apoptotic process (IFIT1, IFIT2, IFIT3, MX1, DDX58, IRF7, XCL2, STAT1, MYD88, RELB, TRAF1, TNFSF10, FASLG, IL-32, CD226, IL2RB, IL15RA) were downregulated (Figures 6A, 6B and Table S8)[26,95]. Many Dex downregulated genes play important roles in promoting NK cell activation, suppressing tumorigenesis and metastasis (Figure 6A and Table S8). For example CD82 suppresses cancer cell invasiveness[96]; interferon induced XAF1 promotes apoptosis of tumor cells[97,98]; CD226 enhances anti-tumor activity of NK cells by inactivating FOXO1, a glucocorticoid induced negative regulator of NK cell function (Figure 6A and Table S8)[53].

The effect of GR activation on cytokine-stimulated NK cells was also investigated. PBMCs were treated with IL-12+IL15+IL18 in the presence or absence of Dex, CD56^{dim}NK cells were sorted and were subjected to bulk RNA-Seq. Again, AREG exhibited the highest fold change in 80 Dex upregulated genes in activated NK cells (Figure 6C and Table S8). A significant overlap of Dex upregulated genes which negatively regulate immune response was observed between cytokine activated NK cells and their counterparts in steady state (Figures 6A, 6C and Table S8). Dex downregulated genes were involved in inflammatory response, lymphocyte activation,

co-stimulation, chemotaxis and anti-tumor activity of NK cells (CD44, TNF, LTA, LTB, CCL5, REL, TRAF1, GPR183, XCL1, XCL2, STAT5A, IL2RB, CD82, TNFRSF9) (Figures 6C, 6D and Table S8)[58,96,99,100]. Thus, GR activation switches the pro-inflammatory characteristics of NK cells to a homeostatic feature, with the most representative signature, AREG upregulation. Next, the effect of supernatant from three states of NK cells (including $AREG^{+}IFN\text{-}\gamma^{-}$, $AREG^{+}IFN\text{-}\gamma^{+}$ and $AREG^{-}IFN\text{-}\gamma^{+}$) on the survival of melanoma cell line (A875) was detected, the survival of A875 was not affected in $AREG^{+}IFN\text{-}\gamma^{-}$ NK cell supernatant, whereas, the percent of live A875 cells was higher in $AREG^{+}IFN\text{-}\gamma^{+}$ than in $AREG^{-}IFN\text{-}\gamma^{+}$ supernatant, suggesting an anti-apoptotic effect of AREG in the presence of IFN-γ (Figure 6E). Since the IFN-γ production between $AREG^{+}IFN\text{-}\gamma^{+}$ and $AREG^{-}IFN\text{-}\gamma^{+}$ NK cells was comparable, the result shown here was unlikely due to the reduced IFN-γ concentration in the supernatant (Figure S5B).

The association of the pro-inflammatory or homeostatic signatures (represented by IFNG or AREG) with cancer survival probability was further interrogated across 31 cancer types in The Cancer Genome Atlas (TCGA, https://cancergenome.nih.gov/). The analysis showed high AREG expression was associated with poor prognosis of multiple cancers across different organs (Figure 6F). However, high IFNG expression was not alway associated with better prognosis in the same cancer types (Figure 6F), suggesting that the homeostatic signature is a more dominant predictor for the prognosis in these cancers.

GR activation induces NK cell memory response in AREG production

Previous study has shown that NK cells possess a memory-like response to inflammatory milieu. NK cells receiving primary inflammatory cytokine stimulation exhibit an enhanced IFN-γ production upon secondary stimulation compared to NK cells without primary stimulation[20,101,102]. Here, we explored whether NK cells exhibit memory response to GR activation, an anti-inflammatory signal. PBMCs receiving primary Dex stimulation or without were rested in low dose IL-15 for 5 days, the production of AREG was undetectable in both groups before secondary stimulation (Figure S5C), after secondary stimulation, the production of AREG between the two groups was compared to measure primary GR activation induced memory response (Figure 7A). Primarily stimulated NK cells uniformly exhibited higher AREG production than their counterparts without primary stimulation (Figures 7B and 7C), indicating NK cells exhibit memory response not only to inflammatory milieu, but also to anti-inflammatory signal.

Our experiment showed IL-15 is not required for Dex induced AREG production within 16 hrs (Figure S5D). After 3 days of Dex treatment, AREG produced by NK cells

were decreased compared with NK cells that were additionally treated with IL-15 (Figure S5D), indicating IL-15 is required for sustained production of AREG induced by Dex. To test whether IL-15 affects Dex induced NK cell memory response, NK cells were additionally treated with high dose IL-15 (Figure 7D), the result showed that IL-15 did not further enhance elevated AREG production due to their memory response to primary GR activation (Figures 7E and 7F).

Next, we tested whether GR activation affects inflammatory cytokine induced NK cell memory response by detecting IFN-γ production using established methods[20,101,102] (Figure 7G). As expected, NK cells receiving IL-12+IL-15+IL-18 primary stimulation exhibited elevated IFN-γ production upon secondary stimulation compared to NK cells without primary stimulation (Figures 7G-7I), however, the memory response was not observed in NK cells that additionally treated with Dex (Figures 8H-8I), suggesting GR activation inhibits inflammatory cytokine induced NK cell memory.

Discussion

NK cells were commonly recognized as innate lymphocytes that play important roles in restricting tumor progression[8]. The transcriptional profile of NK cells in different skin cancers have not been thoroughly characterized and the influence of skin TME on the normal NK cell physiology was not clear, probably due to the large proportion of malignant cells and the limited NK cell numbers in the skin tumor tissue[6,19]. In this study, we specifically enriched $CD45^+$ cells and extracted transcriptome information of NK cells from 24 paired skin tumor and peri-tumor samples using scRNA-Seq (Figure 1A), this effort may also provide valuable resources for investigating other immune cell types in the skin TME.

The transcriptional heterogeneity of skin NK cells was observed in different NK cell clusters (Figure 2C), and this heterogeneity was further shaped by different skin TME (Figures 2 and 3). For example, the signatures of NK cell activation, IFN response, tumor stress and the NK cell cluster unique genes were differentially affected among BCC, cSCC, EMPD and aMM (Figures 2D-2F and 3B-3E). On the other hand, NK cells play important roles in regulating skin TME[25,103,104], and determine the effect of immunotherapy against skin cancer[7]. The concurred up and down regulation of tumor progression related HSP family genes (e.g. DNAJ, HSPA, HSPB, HSPE, HSPH, HSP90)[27,28], and dysregulated NK cell effector function associated genes in the tumor of BCC, EMPD and aMM (Figures 3B-3E) may represent as an immune evasion mechanism in these skin cancers.

We found the skin tumor NK cells commonly upregulated the production of AREG, which play important roles in mediating immune tolerance and promoting tumor growth[11–14], on the contrary, their production of anti-tumor factor TNF-α was suppressed in BCC and cSCC, suggesting an altered microenvironment in these skin tumors switches NK cells anti-tumor activity to a homeostasis feature (Figures 4B-4D). Single cell analysis indicated that the elevated glucocorticoid receptor activity was responsible for the increased AREG production by skin tumor NK cells (Figures 5A-5C and 5F). We showed GR activation specifically induced NK cell AREG production and suppressed their anti-tumor function (Figures 5G-5L and 6A-6D). Considering the facts that high AREG is associated with poor prognosis of multiple cancers (Figure 6F), and GR activation promote tumor metastasis and compromises treatment against cancer[78,79], targeting on glucocorticoid-NR3C1-NK cell-AREG axis may serve as a new strategy to boost the effect of anti-tumor therapy.

Finally, we demonstrated that the primary GR activation induces NK cell memory response of AREG production, on the other hand, the primary pro-inflammatory cytokine induced NK cell memory response of IFN-γ production was suppressed by glucocorticoid treatment (Figures 7A-7C and 7G-7I). This feature may explain the adaptation of reduced dose of glucocorticoid during anti-inflammatory therapy, and failure to form this memory-like response may result in the resistance to glucocorticoid treatment. In general, this study provides new insights on glucocorticoid and NK cell based anti-cancer treatment.

Acknowledgments

We thank the study participants who provided skin and blood samples. Wei Cheng, Hao Chen and Zhiming Chen assisted in acquiring skin cancer and histology pictures. All staff in the biobank of Institute of Dermatology, Chinese Academy of Medical Sciences, Jiangsu Biobank of Clinical Resources assisted with clinical sample collection. Guangzhou Genedenovo Biotechnology Co., Ltd assisted with sequencing data analysis. This study was supported by Hospital for Skin Diseases, Institute of Dermatology, Chinese Academy of Medical Sciences and Peking Union Medical College grant (3301030103119) to Yetao W., National key research and development program (2022YFC2504700, 2022YFC2504701, 2022YFC2504705) to Yan W., The open project of Jiangsu provincial science and technology resources (Clinical Resources) coordination service platform (TC2022B016), The Jiangsu provincial natural science funds for young scholars (SBK2023041928) and The young scientists fund of the national natural science foundation of China (82304236) to Y.L..

Author contributions

Yetao Wang: Conceptualization; experiment design; data analysis; resources; supervision; validation; investigation; visualization; methodology; data curation; software; writing – original draft, review and editing; project administration; funding acquisition. Yan Wang: resources. Qin Wei: performing experiments; data analysis; validation; visualization, data curation. Guirong Liang: performing experiments. Ruizeng: performing experiments; data analysis; validation. Yuancheng Li: data analysis; validation; visualization, software. Anlan Hong: resources. Hongsheng Wang: resources. Suying Feng: resources.

Declaration of interests

All authors declare no competing interests.

Figure legends

Figure 1. NK cells are stable constituents of skin tumor lymphocytes

(A) Experimental design of this study.
(B) UMAP of skin tumor and peri-tumor $CD45^+$ lymphocytes.
(C) The expression of cell type specific markers for (B).
(D) The expression of NK cell and other cell type specific markers in the NK cell cluster.
(E) Flow cytometry of NK cells in tumor and peri-tumor of BCC, cSCC, EMPD and aMM.
(F) Percentage of NK cells in dermal $CD45^+$ cells from skin tumor and peri-tumor.
(G) Number of NK cells per million live dermal cells from skin tumor and peri-tumor.
(H) Percentage of dermal $CD45^+$ cells from skin tumor and peri-tumor.
(I) Number of $CD45^+$ cells per million live dermal cells from skin tumor and peri-tumor.
For (F-I) n=31, each dot represents a unique skin tumor donor (11 BCC, 14 cSCC, 4 EMPD and 2 aMM), Wilcoxon matched-pairs signed rank test, ns, not significant, data are mean with s.e.m. See also Figures S1, S2 and Table S1.

Figure 2. Transcriptional features of NK cells in different skin cancers

(A) UMAP of re-clustered skin tumor and peri-tumor NK cells.
(B) Percentage of NK cell clusters in skin tumor and peri-tumor in different skin cancers.
(C) Representative genes for each NK cell cluster.
(D-F) Gene set score analysis of signatures of NK cell activation (D), IFN response (E) and tumor stress (F) of skin tumor and peri-tumor NK cell clusters of BCC, cSCC, EMPD and aMM. The gene set score was calculated by AddMouduleScore in Seurat, the P value was determined by Wilcoxon rank-sum test using R software.
See also Tables S3 and S4.

Figure 3. NK cell regulon analysis and cluster unique DEgenes of skin cancers
(A) The regulons within each skin cancer were identified by SCENIC (left), the DEregulons between peri-tumor and tumor was determined by two tailed paired t-test based on their average AUCell score (P<0.05, Log2FC>0.5). The transcriptional regulatory networks were visualized by Cytoscape (right), the AUCell score of DEregulons were colored in red or blue representing their up or down regulation in the tumor. The circle area represents the number of DEgenes associated with DEregulon.
(B-E) NK cell cluster unique DEgenes in BCC (B), cSCC (C), EMPD (D) and aMM (E). DEgenes of tumor vs peri-tumor for each NK cell cluster were determined by Seurat FindAllMarkers (P<0.05, Log_2FC>0.36). The cluster unique DEgenes were selected by their Log_2FC value 1.5 fold higher than the other clusters.
See also Tables S6 and S7.

Figure 4. Skin tumor TME upregulates AREG production by NK cells.
(A) The expression of AREG, IFNG and TNF in NK cell clusters.
(B) Skin dermal cells were stimulated with PMA and ionomycin for 3 hrs, the production of AREG, IFN-γ and TNF-α by NK cells ($CD45^+Lin^-TBX21^+$) were detected by flow cytometry.
(C-E) Percentage of $AREG^+$ (C, n=23), TNF-$α^+$ (D, n=21) and IFN-$γ^+$ (E, n=23) NK cells in the tumor and peri-tumor detected in (B),
(F) NK cells from (B) were gated with AREG vs IFN-γ or AREG vs TNF-α.
(G-L) Percentage of $AREG^+$IFN-$γ^-$ (G), $AREG^+$IFN-$γ^+$ (H), $AREG^-$IFN-$γ^+$ (I) NK cells (n=23) and $AREG^+$TNF-$α^-$ (J), $AREG^+$TNF-$α^+$ (K) and $AREG^-$TNF-$α^+$ (L) NK cells (n=21) detected in (F).
(M, N) Correlation of $AREG^-$IFN-$γ^+$ with $AREG^+$IFN-$γ^-$ (M) or with $AREG^+$IFN-$γ^+$ (N) dermal NK cells (n=46).
(O, P) Correlation of $AREG^-$TNF-$α^+$ with $AREG^+$TNF-$α^-$ (O) or with $AREG^+$TNF-$α^+$ (P) dermal NK cells (n=42).
For (C-E), (G-L), each dot represents a unique skin tumor donor, Wilcoxon matched-pairs signed rank test, data are mean with s.e.m., for (M-P), Spearman correlation, ns, not significant.

Figure 5. Glucocorticoid receptor activation induces NK cells AREG production.
(A, B) The average counts of AREG (A) and glucocorticoid target genes (B) between C1, 3, 4, 5 and C0, 2 NK cells. P value was determined by Seurat FindMarkers.
(C) Gene set score between C1, 3, 4, 5 and C0, 2 NK cells as performed in Figure 2D.
(D, E) Pearson correlation of tumor stress score with GR pathway activity score (D) and NK cell activation score (E).
(F) The average counts of glucocorticoid target genes and AREG between skin tumor and peri-tumor C0, 2 NK cells. P value was determined by Seurat FindMarkers.

(G) PMBCs were stimulated with Dex for 16 hrs, the production of AREG in indicated cell populations were detected by flow cytometry.
(H) Percentage of $AREG^+$ cells in (G), n=8, two-tailed paired t-test.
(I) Schematic map of AREG open chromatin region in NK cells (NK cell ATAC-Seq data: GES122548). NR3C1 binding motif was identified by JASPAR motif analysis.
(J) Control, AREG or NR3C1 knockout NK cells were stimulated with Dex for 16 hrs, their AREG production was detected by flow cytometry.
(K) PBMCs were stimulated with Dex or Dex+GR inhibitor (RU486) for 16 hrs, the production of AREG by NK cells was detected by flow cytometry.
(L) Percentage of $AREG^+$NK cells in (K), n=7, two-tailed paired t-test.
For (A-C) and (F) each dot represents a unique skin tumor donor. For (H) and (L), each dot represents a unique PBMC donor.

Figure 6. GR activation induces a homeostatic program of NK cells.
(A) PBMCs were treated with or without Dex in RPMI for 16 hrs, $CD56^{dim}$NK cells were stored and were subjected to bulk RNA-Seq, the DEgenes were shown in volcano plot (Log_2FC> 0.5, P<0.01, determined by DESeq2, n=3).
(B) Enriched pathways of Dex up (red) and down (blue) regulated genes by GO enrichment analysis (FDR<0.05).
(C) As performed in (A), DEgenes of Dex treated or untreated NK cells in the condition of IL-12+IL-15+IL-18 stimulation were shown (n=3).
(D) Enriched pathways of Dex up (red) and down (blue) regulated genes in the condition of IL-12+IL-15+IL-18 stimulation by GO enrichment analysis (FDR<0.05).
(E) After 16 hrs stimulation under indicated conditions, the NK cells were washed for 3 times and were re-cultured in RPMI 1640 for 48 hrs, the supernatants were collected for A875 cell culture for 48 hrs, then cells were digested with trypLE for live/dead staining. Each condition includes 3 repeated, two-tailed paired t-test, ns, not significant, data are mean with s.e.m.
(F) The association of AREG or IFNG expression with the survival probability in different cancer types based on the TCGA database. HR (hazard ratio), Lung Squamous Cell Carcinoma (LUSC), Lung Adenocarcinoma (LUAD), Head-Neck Squamous Cell Carcinoma (HNSC), Acute myeloid leukemia (LAML), Liver Hepatocellular Carcinoma (LIHC), Pancreatic adenocarcinoma (PAAD).

Figure 7. GR activation induces NK cell memory response in AREG production.
(A) Experimental schematic for detecting primary GR activation induced NK cell memory.
(B) PBMCs with or without primary Dex stimulation were secondarily stimulated with Dex, the AREG production by NK cells were detected by flow cytometry.
(C) Percentage of $AREG^+$NK cells in (B) (n=11).

(D) Experimental schematic for detecting the effect of IL-15 on GR activation induced NK cell memory.
(E) AREG production from NK cells was detected as (B), with an additional high dose IL-15 treatment.
(F) Percentage of AREG^{+}NK cells in (E) (n=7).
(G) Experimental schematic for detecting the effect of Dex on pro-inflammatory cytokine induced NK cell memory.
(H) PBMCs without primary stimulation or with IL-12+IL15+IL18 primary stimulation in the presence or absence of Dex, were secondarily stimulated with IL-12+IL15, the IFN-γ production by NK cells were detected by flow cytometry.
(I) Percentage of IFN-γ^{+}NK cells in (H) (n=7).
For (C), (F) and (I), two-tailed paired t-test, data are mean with s.e.m., each dot represents a unique health PBMC donor.

STAR Methods

Key resources table

REAGENT or RESOURCE	SOURCE	IDENTIFIER
Antibodies		
Anti-Human CD3	Biolegend	Cat# 317306
Anti-Human CD4	Biolegend	Cat# 317408
Anti-Human TCRα/β/	Biolegend	Cat# 306706
Anti-Human TCRγ/δ	Biolegend	Cat# 331208
Anti-Human CD19	Biolegend	Cat# 302206
Anti-Human CD20	Biolegend	Cat# 302304
Anti-Human CD22	Biolegend	Cat# 363508
Anti-Human CD14	Biolegend	Cat# 325604
Anti-Human CD34	ebioscience	Cat# 11-0349-42
Anti-Human FcεR1α	ebioscience	Cat# 11-5899-42
Anti-Human CD1a	Biolegend	Cat# 300104
Anti-Human CD11c	Biolegend	Cat# 301604
Anti-Human CD123	Biolegend	Cat# 306014
Anti-Human BDCA2	Biolegend	Cat# 354208
Anti-Human TBX21	ebioscience	Cat# 25-5825-82
Anti-Human IFN-γ	ebioscience	Cat# 17-7319-82
Anti-Human IFN-γ	ebioscience	Cat# 45-7319-42
Anti-Human TNF-α	ebioscience	Cat# 45-7349-42

Anti-Human AREG	ebioscience	Cat# 17-5370-42
Anti-Human CD45	ebioscience	Cat# 56-9459-42
Anti-Human CD56	Biolegend	Cat# 318306
Anti-Human CD56	BD	Cat# 564057
Biological Samples		
PBMCs	Jiangsu province blood center	https://www.jsblood.com.cn/
Chemicals, Peptides, and Recombinant Proteins		
IL-2	Novoprotein	Cat# C013
IL-12	Novoprotein	Cat# CI58
IL-15	Novoprotein	Cat# C016
IL-18	Novoprotein	Cat# CH29
IL-21	Novoprotein	Cat# CC45
4-1BBL	Novoprotein	Cat# CH04
MICA	Novoprotein	Cat# C489
Transferrin	Novoprotein	Cat# CJ41
IGF-I	Novoprotein	Cat# C032
IGF-II	Novoprotein	Cat# CF61
Insulin	Solarbio	Cat# I8830
PMA	Beyotime	Cat# S1819
Ionomycin	Beyotime	Cat# S1672
Mifepristone	MedChemExpress	Cat# HY-13683
Dexamethasone Sodium Phosphate Injection	Shiyao YINHU Pharmaceutical Co., Ltd.	Lot# 1022122362
Methylprednisolone Sodium Succinate	Sinopharm Ronshyn Pharmaceutical Co., Ltd.	LOT# 22101707
Compound Betamethasone Injection	Schering-Plough Labo N.V.	LOT# 00001473561
Cell stimulation cocktail	ebioscience	Cat# 00-4970-03
Protein transport inhibitor	ebioscience	Cat# 00-4980-03
TRIzol reagent	Invitrogen	Cat# 15596026
RNAClean XP	Beckman Culter	Cat# A63987
Alt-R S.p. Cas9 Nuclease V3	Integrated DNA Technologies	Cat# 1081059
ExoSAP-IT	Affymetrix	Cat# 78200
SuperScript™ III Reverse Transcriptase	Invitrogen	Cat# 18080-093

Fixable Viability Dye efluor 780	Invitrogen	Cat# 65-0865-18
Critical Commercial Assays		
Universal DNA purification kit	Tiangen	Cat# DP214-02
Blood genomic DNA isolation kit	Karroten	Cat# K2302
RNA fragmentation reagents	Invitrogen	AM8740
P3 Primary Cell 4D-NucleofectorTM X Kit S	Lonza	Cat# V4XP-3032
EasySep Human NK Cell Isolation Kit	STEMCELL	Cat#17955
NK MACS Medium human	MACS	Cat# 130-114-429
Single Cell 3' Reagent Kits v3.1	10 X Genomics	PN-1000121
NEBNext Ultra II Non directional Second Strand Synthesis Module	NEB	Cat# E6111L
HiScribe T7 High Yield RNA Synthesis Kit	NEB	Cat# E2040S
Deposited Data		
	NCBI Gene Expression Omnibus	
Software and Algorithms		
FlowJo	FlowJo, LLC	https://www.flowjo.com/
GraphPad Prism	GraphPad Software, Inc	https://www.graphpad.com/scientific-software/prism/
Cell Ranger	10x Genomics	https://support.10xgenomics.com/single-cell-gene-expression/software/pipelines/latest/what-is-cell-ranger
SAMtools	Li H. et al.[105]	http://www.htslib.org
R Statistical Computing Software	The R Foundation	https://www.r-project.org/
JASPAR	JASPAR	http://jaspar.genereg.net
DESeq2	Love M. et al.[106]	https://bioconductor.org/packages/release/bioc/html/DESeq2.htmll

GSEA	Subramanian A. et al.[107]	https://www.gsea-msigdb.org/gsea/index.jsp
GSVA	Hänzelmann, S. et al.[108]	https://www.bioconductor.org/packages/release/bioc/html/GSVA.html
Seurat 3.0	Stuart T. et al.[109]	http://satijalab.org/seurat/
SCENIC	Aibar S. et al.[29]	https://github.com/aertslab/SCENIC
Cytoscape	Shannon P. et al.[110]	https://cytoscape.org/
bowtie2	Langmead B. et al.[111]	https://bowtie-bio.sourceforge.net/bowtie2/index.shtml
celseq2	Hashimshony T. et al.[112]	https://github.com/yanailab/celseq2

Resource availability

Further information and requests for resources and reagents should be directed to and will be fulfilled by the lead contact, Yetao Wang (yetaowang@163.com).

Materials availability

This study did not generate new unique reagents.

Data and code availability

The datasets produced in this study, including scRNA-Seq data of skin tumor and peri-tumor, and bulk RNA-Seq data of Dex treated and untreated NK cells, are available in NCBI Gene Expression Omnibus (GEO) with accession number: GSE242941.

Clinical samples

Skin tumor and peri-tumor samples were obtained from the biobank of Institute of Dermatology, Chinese Academy of Medical Sciences, Jiangsu Biobank of Clinical Resources (BM2015004). Blood samples were obtained from Jangsu province blood center. All participants provided written informed consent for protocols that were included in the study of cellular immunity in skin cancers, in accordance with procedures approved by the ethics committee of Institute of Dermatology, Chinese Academy of Medical Sciences and Peking Union Medical College. The clinical characteristics for each donor of skin cancer were provided in Figure S1 and Table S1 .

Human skin cell preparation

Isolation of dermal single cells from peri-tumor and tumor tissues for *in vitro* culture and flow cytometry: 1. After scraping off the subcutaneous fat tissue, skin biopsies were transferred to 1 ml dispase (5 U/mL in PBS containing 1% penicillin/streptomycin) and were incubated in 37°C for 2 hrs to separate epidermis from dermis; 2. Dermis was washed briefly in PBS and was transfer to dermis digestion solution (Collagenase III 3mg/ml + DNase (5 ug/ml) in 10% FBS/RPMI 1640) at 37°C for 2 hrs, shaking vigorously every 30 min; 3. The digested dermis was filtered through a 70 um strainer, the flow through was collected in a 15 ml tube, after centrifuge at 700 x g for 3min, the cells were resuspended in 500 ul MACS buffer (0.5% BSA and 2 mM EDTA in PBS), ready for use.

Isolation of skin $CD45^+$ cells for scRNA-Seq: Skin biopsies were digested according to the instruction of the whole skin dissociation kit (130-101-540, MACS). Briefly, after scraping off fat tissue, skin biopsies were cutted into small pieces (< 4 mm^2), each piece was digested with a buffer containing 435 ul buffer L, 12.5 ul enzyme P, 50 ul enzyme D and 2.5 ul enzyme A on 37°C shaker for 3 hrs. The digested skin tissue was diluted with ice cold DMEM containing 2% BSA, then was filtered through a 70 um strainer, the flow through was centrifuged at 300 x g for 10 min at 4°C. The isolated skin cells were resuspended in MACS buffer and were subjected to $CD45^+$ cell enrichment using magnetic beads (130-045-801, MACS).

Peripheral blood mononuclear cells (PBMCs) isolation

Each human peripheral blood leukopak was washed with 80 ml serum free RPMI 1640 (Gibco), and was overlaid on lymphoprep (STEMSELL, 07851), then was centrifuged at 500 x g for 30 min in room temperature. After washing with MACS buffer for 3 times, the isolated PBMCs were either used immediately or frozen in FBS containing 10% DMSO.

Flow cytometry

Skin cells or PBMCs were first stained with fixable viability dye efluor 780 (Invitrogen, 65-0865-18). For surface staining, cells were incubated in MACS buffer with antibodies at 4°C for 30 min in the dark. For intracellular staining, cells were fixed and permeabilized using Foxp3 staining kit (eBioscience, 00-5523-00), then cytokines or TBX21 were stained with antibodies in the permeabilization buffer at 4°C for 30 min in the dark. After washing with MACS buffer, the cells were ready for flow cytometry detection.

NK cell sorting

PBMCs were stained with fixable viability dye efluor 780, lineage antibodies (against CD3, CD4, TCRαβ, TCRγδ, CD19, CD20, CD22, CD34, FcεRIα, CD11c, CD303,

CD123, CD1a, and CD14) and antibody against CD56. $CD56^{dim}$NK cells were sorted as indicated in Figure S5A using BD FACSAria IIu. The sorted NK cells were subjected to bulk RNA-Seq library preparation using CEL-Seq2.

Cell culture and stimulation conditions

All cells were cultured at 37°C containing 5% CO_2.

Figure 4B-4L: Dermal cells were stimulated with PMA (81 nM) and ionomycin (1.34 uM) (1:500, eBioscience, 00-4970-03) in RPMI 1640 for 2 hrs.

Figure 5G and 5H: PBMCs were stimulated with Dex (100 nM) in RPMI 1640 for 16 hrs.

Figure 5J: After electroporation for 48 hrs, NK cells were stimulated with Dex (100 nM) in RPMI for 16 hrs.

Figure 5K and 5L: PBMCs were stimulated with Dex (100 nM) in the presence or absence of RU486 (100 nM) in RPMI 1640 for 16 hrs.

Figure 6A: PBMCs were stimulated with or without Dex (100 nM) in RPMI 1640 for 16 hrs, then were subjected to NK cell sorting.

Figure 6B: PBMCs were stimulated with IL-12 (10 ng/ml) + IL-15 (50 ng/ml) + IL-18 (50 ng/ml) in the presence or absence of Dex (100 nM) in RPMI 1640 for 16 hrs, then were subjected to NK cell sorting.

Figure 6E: The stimulation conditions for NK cells were illustrated in experimental schematics, A875 cells were cultured in indicated supernatants of NK cell culture for 48 hrs.

Figure 7: the stimulation conditions were illustrated in experimental schematics.

scRNA-Seq library preparation

The scRNA-Seq libraries were prepared by Single Cell 3' Reagent Kits v3.1 (10 x Genomics, PN-1000121). The enriched skin $CD45^{+}$ cells were washed and resuspended in 1 x PBS containing 0.05% BSA. Cell number and viability were measured by trypan blue staining under microscope, cell concentration was adjusted to 1,000-1,500 cells/ul (viability > 90%). Single cell suspension was loaded onto Chromium Controller (10 x Genomics) to participate 8,000–10,000 single cells into gel beads in emulsions (GEMs). The quality of amplified cDNA and final sequencing library were measured by Agilent 2100 Expert (Agilent Technologies).The sequencing depth was controlled around 50,000 mean reads/cell. The libraries were sequenced by Illumina NovaSeq 6000.

Bulk RNA-Seq library preparation

The bulk RNA-Seq libraries of sorted Dex treated and untreated $CD56^{dim}$NK cells were prepared using CEL-Seq2[112]. Total RNA of sorted cells was extracted using TRIzol reagent (ThermoFisher, 15596026). 100 ng RNA for each library was used for first

strand cDNA synthesis using barcoded primers as follows (barcode underlined): Dex untreated repeat 1: 5'-GCCGGTAATACGACTCACTATAGGGAGTTCTACAGTCCGACGATCNNNNNNAGACTCTTTTTTTTTTTTTTTTTTTTTTTTTV-3'; Dex untreated repeat 2: 5'-GCCGGTAATACGACTCACTATAGGGAGTTCTACAGTCCGACGATCNNNNNNCATGAGTTTTTTTTTTTTTTTTTTTTTTTTTV-3'; Dex untreated repeat 3: 5'-GCCGGTAATACGACTCACTATAGGGAGTTCTACAGTCCGACGATCNNNNNNCAGATCTTTTTTTTTTTTTTTTTTTTTTTTTV-3'; Dex treated repeat 1: 5'-GCCGGTAATACGACTCACTATAGGGAGTTCTACAGTCCGACGATCNNNNNNAGCTAGTTTTTTTTTTTTTTTTTTTTTTTTTV-3'; Dex treated repeat 2: 5'-GCCGGTAATACGACTCACTATAGGGAGTTCTACAGTCCGACGATCNNNNNNCATGCATTTTTTTTTTTTTTTTTTTTTTTTTV-3'; Dex treated repeat 3: 5'-GCCGGTAATACGACTCACTATAGGGAGTTCTACAGTCCGACGATCNNNNNNTCACAGTTTTTTTTTTTTTTTTTTTTTTTTTV-3'; Cytokine stimulated, Dex untreated repeat 1: 5'-GCCGGTAATACGACTCACTATAGGGAGTTCTACAGTCCGACGATCNNNNNNAGCTCATTTTTTTTTTTTTTTTTTTTTTTTTV-3'; Cytokine stimulated, Dex untreated repeat 2: 5'-GCCGGTAATACGACTCACTATAGGGAGTTCTACAGTCCGACGATCNNNNNNCATGTCTTTTTTTTTTTTTTTTTTTTTTTTTV-3'; Cytokine stimulated, Dex untreated repeat 3: 5'-GCCGGTAATACGACTCACTATAGGGAGTTCTACAGTCCGACGATCNNNNNNAGGATCTTTTTTTTTTTTTTTTTTTTTTTTTV-3'; Cytokine stimulated, Dex treated repeat 1: 5'-GCCGGTAATACGACTCACTATAGGGAGTTCTACAGTCCGACGATCNNNNNNAGCTTCTTTTTTTTTTTTTTTTTTTTTTTTTV-3'; Cytokine stimulated, Dex treated repeat 2: 5'-GCCGGTAATACGACTCACTATAGGGAGTTCTACAGTCCGACGATCNNNNNNCACTAGTTTTTTTTTTTTTTTTTTTTTTTTTV-3'; Cytokine stimulated, Dex treated repeat 3: 5'-GCCGGTAATACGACTCACTATAGGGAGTTCTACAGTCCGACGATCNNNNNNAGTGCATTTTTTTTTTTTTTTTTTTTTTTTTV-3'. The second strand was synthesized using NEBNext Second Strand Synthesis Module (NEB, E6111L). The dsDNA was purified using RNAClean XP (Beckman Culter, A63987) and was subjected to *in vitro* transcription (IVT) using HiScribe T7 High Yield RNA Synthesis Kit (NEB, E2040S). After ExoSAP-IT (Affymetrix, 78200) treatment, the IVT RNA was fragmented using RNA fragmentation reagents (Invitrogen, AM8740) and was subjected to the second round of reverse transcription using random hexamer: 5'-GCCTTGGCACCCGAGAATTCCANN NNNN-3' The final library was amplified with indexed primers: RP1: 5'-AATGATACGGCGACCACCGAGATCTACACGTTCAGAGTTCTACAGTCCGA-3' and RPI1: 5'-CAAGCAGAAGACGGCATACGAGATCGTGATGTGACTGGAGTTCCTTGGCACCCGAGAATTCCA-3'. After quality check, the purified libraries were sequenced by Illumina NovaSeq 6000.

Cas9 RNP mediated knockout in NK cells

NK cells were isolated from PBMCs using EasySep human NK Cell isolation kit (STEMCELL, 17955) and were expanded in NK MACS medium (MACS, 130-114-429) for 10 days to render NK cells competent for electroporation. 200 pmol sgRNA (synthesized from GenScript) were mixed with 100 pmol Cas9 (IDT, 1081059) for 20 min in room temperature to form RNP. One million NK cells were resuspended in 20 ul 4D nucleofector master mix (82% P3 + 18% supplement 1; Lonza, V4XP-3032), and mixed with Cas9 RNP for electroporation using program CM137. The electroporated NK cells were ready for downstream experiments after culturing in NK MACS medium for 48 hrs. The target site for CD19 knockout (control) was 5'-CTAGGTCCGAAACATTCCAC-3'; for AREG knockout was 5'-GAGGACGGTTCACTACTAGA-3'; and for NR3C1 knockout was 5'-TTACATTGGTCGTACATGCA-3', the corresponding sgRNAs were synthesized from IDT.

scRNA-Seq data processing

An average 9043 cells per sample, 49,004 reads and 1243 median genes per cell were identified by cell ranger (10x Genomics, version 5.0.0) (Table S2). Following alignment, cells meeting the following criterias were retained using Seurat (Version 3.0) and were passed to downstream analysis: (1) nFeature range from 200 to 5900; (2) < 49000 UMIs; (3) < 35% UMIs of mitochondria genes. Potential doublets and multiplets were filtered by DoubletFinder, and 196,278 cells were integrated. The exclusive cell type specific markers were used to further exclude doublets and multiplets. CD45 negative non-hematopoietic cell clusters including keratinocytes (KRT1, KRT5, KRT10, KRT14), fibroblasts (MFAP5, PDPN, PDGFRA, COL1A1), endothelial cells (ACKR1, VWF, PECAM1) and pericytes (RGS5, ACTA2, TAGLN) were also excluded based on their cell type specific markers. Total 146,643 CD45 positive cells were re-clusterd into 8 unique clusters (res=0.5) and NK cell cluster was focused for further analysis.

To identify cluster highly expressed genes, the gene expression values for the cluster of interest was compared with the rest clusters using FindMarkers in Seurat by Model-based Analysis of Single-cell Transcriptomics (MAST) test, the average counts for each cluster were calculated by AverageExpression function.

Regulon analysis

SCENIC analysis (version 1.2.4) was performed to identify transcription factors (TFs) that regulate gene expression for each NK cell cluster in different skin cancers using default parameters. Hg19 was downloaded by RcisTarget (version 1.14.0) for reference. Gene regulatory networks were inferred using GENIE3 (version 1.16.0), the enriched TF binding motifs and their predicted target genes (regulons), and the activity of regulons were inferred by AUCell (version 1.16.0). The altered activity of regulons (DEregulons)

between peri-tumor and tumor NK cell clusters were calculated based on their average AUCell scores by two tailed paired t-test (P<0.05, Log_2FC>0.5) and their transcription regulatory networks were visualized by Cytoscape (version 3.5.1).

Gene sets score analysis

The AddModuleScore function in Seurat was used to calculate the gene set score of NK cell clusters, and the significance was determined by Wilcoxon rank-sum test.

Gene set correlation analysis

The AUCell score of each gene set, including GR pathway activity, tumor stress or NK cell activity, in each cell were calculated, the correlation among gene sets was calculated by Pearson correlation. Cells with extreme values (count = 0) were discarded from the analysis.

Bulk RNA-Seq analysis

The transcriptome count matrix of all samples was generated using the default settings of CEL-Seq2 pipeline (https://github.com/yanailab/celseq2)[112]. Briefly, Read 2 was assigned to each sample based on their paired read 1 barcode and was mapped to hg19 using Bowie2. The UMIs for each sample were counted, and the generated count matrix was analyzed by DEseq2 package in R. The counts of transcripts per sample were normalized using variance stabilizing transformation (VST) method in DESeq2. The DEgenes were determined by DEseq2 (Log_2FC> 0.5, P<0.01).

Survival probability analysis

Survival and RNA-seq data from TCGA (The Cancer Genome Atlas) PanCancer project were extracted from the UCSC XENA database (https://xena.ucsc.edu/). The Survival package was to compute Kaplan Meier curves for each tumor and to calculate the log-rank test to obtain the survival probability.

Supplemental Figure legends

Figure S1. Histological pictures of skin cancer donors.

Selected histological pictures of skin cancer donors for BCC (n=13), cSCC (n=15), EMPD (n=5) and aMM (n=4).

Figure S2. Detection of NK cells by scRNA-Seq.

(A) The expression of markers for NK and other cell types in NK cells clusters.

(B) The distribution of NK cells from different skin tumor and peri-tumor donors.

Figure S3. Detection of NK cells by flow cytometry.
(A) The number of DEgenes between skin tumor and peri-tumor NK cells in different NK cell clusters from BCC, cSCC, EMPD and aMM.
(B) Skin dermal cells were stimulated with PMA and ionomycin for 3 hrs, the production of AREG, IFN-γ and TNF-α by NK cells ($CD45^{+}Lin^{-}TBX21^{+}$) from BCC, cSCC, EMPD and aMM were detected by flow cytometry. Each dot represents a unique skin tumor donor. Two-tailed paired t-test, data are mean with s.e.m..

Figure S4. Glucocorticoid stimulation induces NK cell AREG production.
(A) PBMCs were stimulated in indicated conditions for 16 hrs, the AREG production from NK cells ($Lin^{-}TBX21^{+}$) were detected using flow cytometry.
(B-C) PBMCs were stimulated in different dose of Betamethasone (B) and Methylprednisolone (C) for 16 hrs, the AREG production from NK cells ($Lin^{-}TBX21^{+}$) were detected using flow cytometry.

Figure S5. NK cells sorting and stimulation.
(A) Purity check of NK cells before and after sorting.
(B) Magnetic beads purified NK cells were cultured in NK MACS medium for 11 days, then were rested in RPMI for 3 days, after stimulating with indicated conditions for 16 hrs as Figure 6E, the production of AREG and IFN-γ was detected in indicated groups.
(C) PBMCs with or without primary Dex stimulation were cultured in low dose IL-15 for 5 days, before secondary Dex stimulation, the production of AREG by NK cells were detected by flow cytometry.
(D) PBMCs were stimulated with or without Dex in the presence or absence of IL-15 for 16 hrs or 3 days, the AREG produced by NK cells were detected by flow cytometry (n=5), two-tailed paired t-test, data are mean with s.e.m., each dot represents a unique health PBMC donor.

References

1. Arnold, M., Singh, D., Laversanne, M., Vignat, J., Vaccarella, S., Meheus, F., Cust, A.E., de Vries, E., Whiteman, D.C., and Bray, F. (2022). Global Burden of Cutaneous Melanoma in 2020 and Projections to 2040. JAMA Dermatol. *158*, 495–503.

2. Henrikson, N.B., Ivlev, I., Blasi, P.R., Nguyen, M.B., Senger, C.A., Perdue, L.A., and Lin, J.S. (2023). Skin Cancer Screening: Updated Evidence Report and Systematic Review for the US Preventive Services Task Force. JAMA *329*, 1296–1307.

3. Tanese, K., Nakamura, Y., Hirai, I., and Funakoshi, T. (2019). Updates on the Systemic Treatment of Advanced Non-melanoma Skin Cancer. Front. Med. *6*, 160.

4. Stonesifer, C.J., Djavid, A.R., Grimes, J.M., Khaleel, A.E., Soliman, Y.S., Maisel-Campbell, A., Garcia-Saleem, T.J., Geskin, L.J., and Carvajal, R.D. (2021). Immune Checkpoint Inhibition in Non-Melanoma Skin Cancer: A Review of Current Evidence. Front. Oncol. *11*, 734354.

5. Jenkins, R.W., and Fisher, D.E. (2021). Treatment of Advanced Melanoma in 2020 and Beyond. J. Invest. Dermatol. *141*, 23–31.

6. Ji, A.L., Rubin, A.J., Thrane, K., Jiang, S., Reynolds, D.L., Meyers, R.M., Guo, M.G., George, B.M., Mollbrink, A., Bergenstråhle, J., et al. (2020). Multimodal Analysis of Composition and Spatial Architecture in Human Squamous Cell Carcinoma. Cell *182*, 1661–1662.

7. Barry, K.C., Hsu, J., Broz, M.L., Cueto, F.J., Binnewies, M., Combes, A.J., Nelson, A.E., Loo, K., Kumar, R., Rosenblum, M.D., et al. (2018). A natural killer–dendritic cell axis defines checkpoint therapy–responsive tumor microenvironments. Nat. Med. *24*, 1178–1191.

8. Laskowski, T.J., Biederstädt, A., and Rezvani, K. (2022). Natural killer cells in antitumour adoptive cell immunotherapy. Nat. Rev. Cancer *22*, 557–575.

9. Basar, R., Daher, M., and Rezvani, K. (2020). Next-generation cell therapies: the emerging role of CAR-NK cells. Hematology Am. Soc. Hematol. Educ. Program *2020*, 570–578.

10. Luci, C., Bihl, F., Bourdely, P., Khou, S., Popa, A., Meghraoui-Kheddar, A., Vermeulen, O., Elaldi, R., Poissonnet, G., Sudaka, A., et al. (2021). Cutaneous Squamous Cell Carcinoma Development Is Associated with a Temporal Infiltration of ILC1 and NK Cells with Immune Dysfunctions. J. Invest. Dermatol. *141*, 2369–2379.

11. Zaiss, D.M.W., Gause, W.C., Osborne, L.C., and Artis, D. (2015). Emerging functions of amphiregulin in orchestrating immunity, inflammation, and tissue repair. Immunity *42*, 216–226.

12. Wang, S., Zhang, Y., Wang, Y., Ye, P., Li, J., Li, H., Ding, Q., and Xia, J. (2016). Amphiregulin Confers Regulatory T Cell Suppressive Function and Tumor Invasion via the EGFR/GSK-3β/Foxp3 Axis. J. Biol. Chem. *291*, 21085–21095.

13. Xu, Q., Long, Q., Zhu, D., Fu, D., Zhang, B., Han, L., Qian, M., Guo, J., Xu, J., Cao, L., et al. (2019). Targeting amphiregulin (AREG) derived from senescent stromal cells diminishes cancer resistance and averts programmed cell death 1 ligand (PD-L1)-mediated immunosuppression. Aging Cell *18*, e13027.

14. Florentin, J., Zhao, J., Tai, Y.-Y., Sun, W., Ohayon, L.L., O'Neil, S.P., Arunkumar, A., Zhang, X., Zhu, J., Al Aaraj, Y., et al. (2022). Loss of Amphiregulin drives inflammation and endothelial apoptosis in pulmonary hypertension. Life Sci Alliance *5*. 10.26508/lsa.202101264.

15. Lindzen, M., Ghosh, S., Noronha, A., Drago, D., Nataraj, N.B., Leitner, O., Carvalho, S., Zmora, E., Sapoznik, S., Shany, K.B., et al. (2021). Targeting autocrine amphiregulin robustly and reproducibly inhibits ovarian cancer in a syngeneic model: roles for wildtype p53. Oncogene *40*, 3665–3679.

16. Hsieh, M.-J., Chen, Y.-H., Lee, I.-N., Huang, C., Ku, Y.-J., and Chen, J.-C. (2019). Secreted amphiregulin promotes vincristine resistance in oral squamous cell carcinoma. Int. J. Oncol. *55*, 949–959.

17. Ishikawa, N., Daigo, Y., Takano, A., Taniwaki, M., Kato, T., Hayama, S., Murakami, H., Takeshima, Y., Inai, K., Nishimura, H., et al. (2005). Increases of amphiregulin and transforming growth factor-alpha in serum as predictors of poor response to gefitinib among patients with advanced non-small cell lung cancers. Cancer Res. *65*, 9176–9184.

18. Wang, Y., Lifshitz, L., Silverstein, N.J., Mintzer, E., Luk, K., StLouis, P., Brehm, M.A., Wolfe, S.A., Deeks, S.G., and Luban, J. (2023). Transcriptional and chromatin profiling of human blood innate lymphoid cell subsets sheds light on HIV-1 pathogenesis. EMBO J., e114153.

19. Guerrero-Juarez, C.F., Lee, G.H., Liu, Y., Wang, S., Karikomi, M., Sha, Y., Chow, R.Y., Nguyen, T.T.L., Iglesias, V.S., Aasi, S., et al. (2022). Single-cell analysis of human basal cell carcinoma reveals novel regulators of tumor growth and the tumor microenvironment. Sci Adv *8*, eabm7981.

20. Wang, Y., Lifshitz, L., Gellatly, K., Vinton, C.L., Busman-Sahay, K., McCauley, S., Vangala, P., Kim, K., Derr, A., Jaiswal, S., et al. (2020). HIV-1-induced cytokines deplete homeostatic innate lymphoid cells and expand TCF7-dependent memory NK cells. Nat. Immunol. *21*, 274–286.

21. Reynolds, G., Vegh, P., Fletcher, J., Poyner, E.F.M., Stephenson, E., Goh, I., Botting, R.A., Huang, N., Olabi, B., Dubois, A., et al. (2021). Developmental cell programs are co-opted in inflammatory skin disease. Science *371*. 10.1126/science.aba6500.

22. Bal, S.M., Golebski, K., and Spits, H. (2020). Plasticity of innate lymphoid cell subsets. Nat. Rev. Immunol. *20*, 552–565.

23. Collins, P.L., Cella, M., Porter, S.I., Li, S., Gurewitz, G.L., Hong, H.S., Johnson, R.P., Oltz, E.M., and Colonna, M. (2019). Gene Regulatory Programs Conferring Phenotypic Identities to Human NK Cells. Cell *176*, 348–360.e12.

24. Tang, F., Li, J., Qi, L., Liu, D., Bo, Y., Qin, S., Miao, Y., Yu, K., Hou, W., Li, J., et al. (2023). A pan-cancer single-cell panorama of human natural killer cells. Cell *0*. 10.1016/j.cell.2023.07.034.

25. de Andrade, L.F., Lu, Y., Luoma, A., Ito, Y., Pan, D., Pyrdol, J.W., Yoon, C.H., Yuan, G.-C., and Wucherpfennig, K.W. (2019). Discovery of specialized NK cell populations infiltrating human melanoma metastases. JCI Insight *4*. 10.1172/jci.insight.133103.

26. Platanias, L.C. (2005). Mechanisms of type-I- and type-II-interferon-mediated signalling. Nat. Rev. Immunol. *5*, 375–386.

27. Albakova, Z., Siam, M.K.S., Sacitharan, P.K., Ziganshin, R.H., Ryazantsev, D.Y., and Sapozhnikov, A.M. (2021). Extracellular heat shock proteins and cancer: New perspectives. Transl. Oncol. *14*, 100995.

28. Liu, X., Li, K., Wang, L., Zhang, M., and Wang, X. (2021). Variations of human heat shock proteins in multiple cancers. Clin. Transl. Med. *11*, e320.

29. Aibar, S., González-Blas, C.B., Moerman, T., Huynh-Thu, V.A., Imrichova, H., Hulselmans, G., Rambow, F., Marine, J.-C., Geurts, P., Aerts, J., et al. (2017). SCENIC: single-cell regulatory network inference and clustering. Nat. Methods *14*, 1083–1086.

30. Narni-Mancinelli, E., Jaeger, B.N., Bernat, C., Fenis, A., Kung, S., De Gassart, A., Mahmood, S., Gut, M., Heath, S.C., Estellé, J., et al. (2012). Tuning of natural killer cell reactivity by NKp46 and Helios calibrates T cell responses. Science *335*, 344–348.

31. Bernard, K., Cambiaggi, A., Guia, S., Bertucci, F., Granjeaud, S., Tagett, R., N'Guyen, C., Jordan, B.R., and Vivier, E. (1999). Engagement of natural cytotoxicity programs regulates AP-1 expression in the NKL human NK cell line. J. Immunol. *162*, 4062–4068.

32. Campbell, N.K., Fitzgerald, H.K., and Dunne, A. (2021). Regulation of inflammation by the antioxidant haem oxygenase 1. Nat. Rev. Immunol. *21*, 411–425.

33. Ni, L., Wang, L., Yao, C., Ni, Z., Liu, F., Gong, C., Zhu, X., Yan, X., Watowich, S.S., Lee, D.A., et al. (2017). The histone deacetylase inhibitor valproic acid inhibits NKG2D expression in natural killer cells through suppression of STAT3 and HDAC3. Sci. Rep. *7*, 45266.

34. Ni, J., Wang, X., Stojanovic, A., Zhang, Q., Wincher, M., Bühler, L., Arnold, A., Correia, M.P., Winkler, M., Koch, P.-S., et al. (2020). Single-Cell RNA Sequencing of Tumor-Infiltrating NK Cells Reveals that Inhibition of Transcription Factor HIF-1α Unleashes NK Cell Activity. Immunity *52*, 1075–1087.e8.

35. Mohamed-Hadley, A.A., and Liebermann, D. (2010). Stress Response Gadd45a Gene Functions as Tumor Suppressor In MYC Expressing Myeloid Cells Modulating Apoptosis and Cytokine Receptor Expression. Blood *116*, 1556.

36. Zhou, R., Tardivel, A., Thorens, B., Choi, I., and Tschopp, J. (2010). Thioredoxin-interacting protein links oxidative stress to inflammasome activation. Nat. Immunol. *11*, 136–140.

37. Maifrede, S., Liebermann, D., and Hoffman, B. (2014). Egr-1, a Stress Response Transcription Factor and Myeloid Differentiation Primary Response Gene, Behaves As Tumor Suppressor in CML. Blood *124*, 2211–2211.

38. Wang, J., Zhou, J.-Y., Kho, D., Reiners, J.J., Jr, and Wu, G.S. (2016). Role for DUSP1 (dual-specificity protein phosphatase 1) in the regulation of autophagy. Autophagy *12*, 1791–1803.

39. Qin, C., Liu, S., Zhou, S., Wang, Q., Xia, X., Hu, J., Yuan, X., Wang, Z., Yu, Y., and Ma, D. (2023). PIK3C2A is a prognostic biomarker that is linked to immune infiltrates in kidney renal clear cell carcinoma. Front. Immunol. *14*, 1114572.

40. Cao, Z., Sun, X., Icli, B., Wara, A.K., and Feinberg, M.W. (2010). Role of Kruppel-like factors in leukocyte development, function, and disease. Blood *116*, 4404–4414.

41. Cheng, M.I., Li, J.H., Riggan, L., Chen, B., Tafti, R.Y., Chin, S., Ma, F., Pellegrini, M., Hrncir, H., Arnold, A.P., et al. (2023). The X-linked epigenetic regulator UTX controls NK cell-intrinsic sex differences. Nat. Immunol. *24*, 780–791.

42. Whang, M.I., Tavares, R.M., Benjamin, D.I., Kattah, M.G., Advincula, R., Nomura, D.K.,

Debnath, J., Malynn, B.A., and Ma, A. (2017). The ubiquitin binding protein TAX1BP1 mediates autophagosome induction and the metabolic transition of activated T cells. Immunity *46*, 405–420.

43. Sedlyarov, V., Eichner, R., Girardi, E., Essletzbichler, P., Goldmann, U., Nunes-Hasler, P., Srndic, I., Moskovskich, A., Heinz, L.X., Kartnig, F., et al. (2018). The Bicarbonate Transporter SLC4A7 Plays a Key Role in Macrophage Phagosome Acidification. Cell Host Microbe *23*, 766–774.e5.

44. Holmes, T.D., Wilson, E.B., Black, E.V.I., Benest, A.V., Vaz, C., Tan, B., Tanavde, V.M., and Cook, G.P. (2014). Licensed human natural killer cells aid dendritic cell maturation via TNFSF14/LIGHT. Proc. Natl. Acad. Sci. U. S. A. *111*, E5688–E5696.

45. Loftus, R.M., Assmann, N., Kedia-Mehta, N., O'Brien, K.L., Garcia, A., Gillespie, C., Hukelmann, J.L., Oefner, P.J., Lamond, A.I., Gardiner, C.M., et al. (2018). Amino acid-dependent cMyc expression is essential for NK cell metabolic and functional responses in mice. Nat. Commun. *9*, 2341.

46. Siggs, O.M., Li, X., Xia, Y., and Beutler, B. (2012). ZBTB1 is a determinant of lymphoid development. J. Exp. Med. *209*, 19–27.

47. Chen, J.C., Perez-Lorenzo, R., Saenger, Y.M., Drake, C.G., and Christiano, A.M. (2018). IKZF1 Enhances Immune Infiltrate Recruitment in Solid Tumors and Susceptibility to Immunotherapy. Cell Syst *7*, 92–103.e4.

48. Mizesko, M.C., Banerjee, P.P., Monaco-Shawver, L., Mace, E.M., Bernal, W.E., Sawalle-Belohradsky, J., Belohradsky, B.H., Heinz, V., Freeman, A.F., Sullivan, K.E., et al. (2013). Defective actin accumulation impairs human natural killer cell function in patients with dedicator of cytokinesis 8 deficiency. J. Allergy Clin. Immunol. *131*, 840–848.

49. Li, Z.-Y., Morman, R.E., Hegermiller, E., Sun, M., Bartom, E.T., Maienschein-Cline, M., Sigvardsson, M., and Kee, B.L. (2021). The transcriptional repressor ID2 supports natural killer cell maturation by controlling TCF1 amplitude. J. Exp. Med. *218*. 10.1084/jem.20202032.

50. Wex, T., Wex, H., Hartig, R., Wilhelmsen, S., and Malfertheiner, P. (2003). Functional involvement of cathepsin W in the cytotoxic activity of NK-92 cells. FEBS Lett. *552*, 115–119.

51. Gil-Krzewska, A., Saeed, M.B., Oszmiana, A., Fischer, E.R., Lagrue, K., Gahl, W.A., Introne, W.J., Coligan, J.E., Davis, D.M., and Krzewski, K. (2018). An actin cytoskeletal barrier inhibits lytic granule release from natural killer cells in patients with Chediak-Higashi syndrome. J. Allergy Clin. Immunol. *142*, 914–927.e6.

52. Mounce, B.C., Poirier, E.Z., Passoni, G., Simon-Loriere, E., Cesaro, T., Prot, M., Stapleford, K.A., Moratorio, G., Sakuntabhai, A., Levraud, J.-P., et al. (2016). Interferon-Induced Spermidine-Spermine Acetyltransferase and Polyamine Depletion Restrict Zika and Chikungunya Viruses. Cell Host Microbe *20*, 167–177.

53. Du, X., de Almeida, P., Manieri, N., de Almeida Nagata, D., Wu, T.D., Harden Bowles, K., Arumugam, V., Schartner, J., Cubas, R., Mittman, S., et al. (2018). CD226 regulates natural killer cell antitumor responses via phosphorylation-mediated inactivation of transcription

factor FOXO1. Proc. Natl. Acad. Sci. U. S. A. *115*, E11731–E11740.

54. Lopes, I.A., Kardosova, M., Bianco, T.M., Arantes, A.Q., Silva, C.A., Scheucher, P.S., Tenen, D.G., Lee, S., Rego, E.M., Welner, R.S., et al. (2018). C/Ebpg (CCAAT/Enhancer Binding Protein Gamma) Balances Cytotoxic and Secretory Potential of Natural Killer Cells. Blood *132*, 3721–3721.

55. Rapp, M., Lau, C.M., Adams, N.M., Weizman, O.-E., O'Sullivan, T.E., Geary, C.D., and Sun, J.C. (2017). Core-binding factor β and Runx transcription factors promote adaptive natural killer cell responses. Sci Immunol *2*. 10.1126/sciimmunol.aan3796.

56. Lanier, L.L. (2009). DAP10- and DAP12-associated receptors in innate immunity. Immunol. Rev. *227*, 150–160.

57. Turnbull, I.R., and Colonna, M. (2007). Activating and inhibitory functions of DAP12. Nat. Rev. Immunol. *7*, 155–161.

58. Galandrini, R., De Maria, R., Piccoli, M., Frati, L., and Santoni, A. (1994). CD44 triggering enhances human NK cell cytotoxic functions. J. Immunol. *153*, 4399–4407.

59. Ma, S., Han, J., Li, Z., Xiao, S., Zhang, J., Yan, J., Tang, T., Barr, T., Kraft, A.S., Caligiuri, M.A., et al. (2023). An XBP1s-PIM-2 positive feedback loop controls IL-15-mediated survival of natural killer cells. Sci Immunol *8*, eabn7993.

60. Cacalano, N.A. (2016). Regulation of Natural Killer Cell Function by STAT3. Front. Immunol. *7*, 128.

61. Liu, L.L., Landskron, J., Ask, E.H., Enqvist, M., Sohlberg, E., Traherne, J.A., Hammer, Q., Goodridge, J.P., Larsson, S., Jayaraman, J., et al. (2016). Critical Role of CD2 Co-stimulation in Adaptive Natural Killer Cell Responses Revealed in NKG2C-Deficient Humans. Cell Rep. *15*, 1088–1099.

62. Masuyama, J.-I., Murakami, T., Iwamoto, S., and Fujita, S. (2016). Ex vivo expansion of natural killer cells from human peripheral blood mononuclear cells co-stimulated with anti-CD3 and anti-CD52 monoclonal antibodies. Cytotherapy *18*, 80–90.

63. Miyake, T., Satoh, T., Kato, H., Matsushita, K., Kumagai, Y., Vandenbon, A., Tani, T., Muta, T., Akira, S., and Takeuchi, O. (2010). IκBζ is essential for natural killer cell activation in response to IL-12 and IL-18. Proc. Natl. Acad. Sci. U. S. A. *107*, 17680–17685.

64. Demir, S., Wolff, G., Wieder, A., Maida, A., Bühler, L., Brune, M., Hautzinger, O., Feuchtinger, A., Poth, T., Szendroedi, J., et al. (2022). TSC22D4 interacts with Akt1 to regulate glucose metabolism. Sci Adv *8*, eabo5555.

65. Holmes, M.L., Huntington, N.D., Thong, R.P.L., Brady, J., Hayakawa, Y., Andoniou, C.E., Fleming, P., Shi, W., Smyth, G.K., Degli-Esposti, M.A., et al. (2014). Peripheral natural killer cell maturation depends on the transcription factor Aiolos. EMBO J. *33*, 2721–2734.

66. Taveirne, S., Wahlen, S., Van Loocke, W., Kiekens, L., Persyn, E., Van Ammel, E., De Mulder, K., Roels, J., Tilleman, L., Aumercier, M., et al. (2020). The transcription factor ETS1 is an important regulator of human NK cell development and terminal differentiation. Blood *136*, 288–298.

67. Höfle, J., Trenkner, T., Kleist, N., Schwane, V., Vollmers, S., Barcelona, B., Niehrs, A., Fittje, P., Huynh-Tran, V.H., Sauter, J., et al. (2022). Engagement of TRAIL triggers degranulation and IFNγ production in human natural killer cells. EMBO Rep. *23*, e54133.

68. Shi, D., Wu, X., Jian, Y., Wang, J., Huang, C., Mo, S., Li, Y., Li, F., Zhang, C., Zhang, D., et al. (2022). USP14 promotes tryptophan metabolism and immune suppression by stabilizing IDO1 in colorectal cancer. Nat. Commun. *13*, 5644.

69. Buechele, C., Baessler, T., Wirths, S., Schmohl, J.U., Schmiedel, B.J., and Salih, H.R. (2012). Glucocorticoid-induced TNFR-related protein (GITR) ligand modulates cytokine release and NK cell reactivity in chronic lymphocytic leukemia (CLL). Leukemia *26*, 991–1000.

70. Sakurai, T., Okuyama, Y., Kobayashi, S., Phung, H.T., Asao, A., Kawabe, T., Ndhlovu, L.C., Riccardi, C., Kudo, H., Wada, M., et al. (2020). GITR controls intestinal inflammation by suppressing IL-15-dependent NK cell activity. FASEB J. *34*, 14820–14831.

71. Duygu, B., Olieslagers, T.I., Groeneweg, M., Voorter, C.E.M., and Wieten, L. (2021). HLA Class I Molecules as Immune Checkpoints for NK Cell Alloreactivity and Anti-Viral Immunity in Kidney Transplantation. Front. Immunol. *12*, 680480.

72. Coutinho, A.E., and Chapman, K.E. (2011). The anti-inflammatory and immunosuppressive effects of glucocorticoids, recent developments and mechanistic insights. Mol. Cell. Endocrinol. *335*, 2–13.

73. Khadka, S., Druffner, S.R., Duncan, B.C., and Busada, J.T. (2023). Glucocorticoid regulation of cancer development and progression. Front. Endocrinol. *14*, 1161768.

74. Stoll, S.W., Stuart, P.E., Lambert, S., Gandarillas, A., Rittié, L., Johnston, A., and Elder, J.T. (2016). Membrane-Tethered Intracellular Domain of Amphiregulin Promotes Keratinocyte Proliferation. J. Invest. Dermatol. *136*, 444–452.

75. Zhao, X., Yang, W., Yu, T., Yu, Y., Cui, X., Zhou, Z., Yang, H., Yu, Y., Bilotta, A.J., Yao, S., et al. (2023). Th17 Cell-Derived Amphiregulin Promotes Colitis-Associated Intestinal Fibrosis Through Activation of mTOR and MEK in Intestinal Myofibroblasts. Gastroenterology *164*, 89–102.

76. Wang, J.-C., Derynck, M.K., Nonaka, D.F., Khodabakhsh, D.B., Haqq, C., and Yamamoto, K.R. (2004). Chromatin immunoprecipitation (ChIP) scanning identifies primary glucocorticoid receptor target genes. Proc. Natl. Acad. Sci. U. S. A. *101*, 15603–15608.

77. Mostafa, M.M., Rider, C.F., Shah, S., Traves, S.L., Gordon, P.M.K., Miller-Larsson, A., Leigh, R., and Newton, R. (2019). Glucocorticoid-driven transcriptomes in human airway epithelial cells: commonalities, differences and functional insight from cell lines and primary cells. BMC Med. Genomics *12*, 29.

78. Yang, H., Xia, L., Chen, J., Zhang, S., Martin, V., Li, Q., Lin, S., Chen, J., Calmette, J., Lu, M., et al. (2019). Stress–glucocorticoid–TSC22D3 axis compromises therapy-induced antitumor immunity. Nat. Med. *25*, 1428–1441.

79. Obradović, M.M.S., Hamelin, B., Manevski, N., Couto, J.P., Sethi, A., Coissieux, M.-M., Münst, S., Okamoto, R., Kohler, H., Schmidt, A., et al. (2019). Glucocorticoids promote

breast cancer metastasis. Nature *567*, 540–544.

80. Uche, U.U., Piccirillo, A.R., Kataoka, S., Grebinoski, S.J., D'Cruz, L.M., and Kane, L.P. (2018). PIK3IP1/TrIP restricts activation of T cells through inhibition of PI3K/Akt. J. Exp. Med. *215*, 3165–3179.

81. Chen, S., Bonifati, S., Qin, Z., St Gelais, C., Kodigepalli, K.M., Barrett, B.S., Kim, S.H., Antonucci, J.M., Ladner, K.J., Buzovetsky, O., et al. (2018). SAMHD1 suppresses innate immune responses to viral infections and inflammatory stimuli by inhibiting the NF-κB and interferon pathways. Proc. Natl. Acad. Sci. U. S. A. *115*, E3798–E3807.

82. Ramasamy, S., Saez, B., Mukhopadhyay, S., Ding, D., Ahmed, A.M., Chen, X., Pucci, F., Yamin, R. 'e, Wang, J., Pittet, M.J., et al. (2016). Tle1 tumor suppressor negatively regulates inflammation in vivo and modulates NF-κB inflammatory pathway. Proc. Natl. Acad. Sci. U. S. A. *113*, 1871–1876.

83. Chodaparambil, J.V., Pate, K.T., Hepler, M.R.D., Tsai, B.P., Muthurajan, U.M., Luger, K., Waterman, M.L., and Weis, W.I. (2014). Molecular functions of the TLE tetramerization domain in Wnt target gene repression. EMBO J. *33*, 719–731.

84. Kim, D.O., Byun, J.-E., Kim, W.S., Kim, M.J., Choi, J.H., Kim, H., Choi, E., Kim, T.-D., Yoon, S.R., Noh, J.-Y., et al. (2020). TXNIP Regulates Natural Killer Cell-Mediated Innate Immunity by Inhibiting IFN-γ Production during Bacterial Infection. Int. J. Mol. Sci. *21*. 10.3390/ijms21249499.

85. Park, A., Lee, Y., Kim, M.S., Kang, Y.J., Park, Y.-J., Jung, H., Kim, T.-D., Lee, H.G., Choi, I., and Yoon, S.R. (2018). Prostaglandin E2 Secreted by Thyroid Cancer Cells Contributes to Immune Escape Through the Suppression of Natural Killer (NK) Cell Cytotoxicity and NK Cell Differentiation. Front. Immunol. *9*, 1859.

86. Cook, M.E., Bradstreet, T.R., Webber, A.M., Kim, J., Santeford, A., Harris, K.M., Murphy, M.K., Tran, J., Abdalla, N.M., Schwarzkopf, E.A., et al. (2022). The ZFP36 family of RNA binding proteins regulates homeostatic and autoreactive T cell responses. Sci Immunol *7*, eabo0981.

87. Bellone, S., Roque, D., Cocco, E., Gasparrini, S., Bortolomai, I., Buza, N., Abu-Khalaf, M., Silasi, D.-A., Ratner, E., Azodi, M., et al. (2012). Downregulation of membrane complement inhibitors CD55 and CD59 by siRNA sensitises uterine serous carcinoma overexpressing Her2/neu to complement and antibody-dependent cell cytotoxicity in vitro: implications for trastuzumab-based immunotherapy. Br. J. Cancer *106*, 1543–1550.

88. Deng, Y., Kerdiles, Y., Chu, J., Yuan, S., Wang, Y., Chen, X., Mao, H., Zhang, L., Zhang, J., Hughes, T., et al. (2015). Transcription factor Foxo1 is a negative regulator of natural killer cell maturation and function. Immunity *42*, 457–470.

89. Akman, B., Hu, X., Liu, X., Hatipoğlu, T., You, H., Chan, W.C., and Küçük, C. (2021). PRDM1 decreases sensitivity of human NK cells to IL2-induced cell expansion by directly repressing CD25 (IL2RA). J. Leukoc. Biol. *109*, 901–914.

90. Smith, M.A., Maurin, M., Cho, H.I., Becknell, B., Freud, A.G., Yu, J., Wei, S., Djeu, J., Celis, E., Caligiuri, M.A., et al. (2010). PRDM1/Blimp-1 controls effector cytokine production in human NK cells. J. Immunol. *185*, 6058–6067.

91. Franco, L.M., Gadkari, M., Howe, K.N., Sun, J., Kardava, L., Kumar, P., Kumari, S., Hu, Z., Fraser, I.D.C., Moir, S., et al. (2019). Immune regulation by glucocorticoids can be linked to cell type-dependent transcriptional responses. J. Exp. Med. *216*, 384–406.

92. Bergeron, B.P., Barnett, K.R., Bhattarai, K.R., Mobley, R.J., Hansen, B.S., Brown, A., Kodali, K., High, A.A., Jeha, S., Pui, C.-H., et al. (2023). Mutual antagonism between glucocorticoid and canonical Wnt signaling pathways in B-cell acute lymphoblastic leukemia. Blood Adv. 10.1182/bloodadvances.2022009498.

93. Schmidleithner, L., Thabet, Y., Schönfeld, E., Köhne, M., Sommer, D., Abdullah, Z., Sadlon, T., Osei-Sarpong, C., Subbaramaiah, K., Copperi, F., et al. (2019). Enzymatic Activity of HPGD in Treg Cells Suppresses Tconv Cells to Maintain Adipose Tissue Homeostasis and Prevent Metabolic Dysfunction. Immunity *50*, 1232–1248.e14.

94. Kalinski, P. (2012). Regulation of immune responses by prostaglandin E2. J. Immunol. *188*, 21–28.

95. Liu, S.-Y., Sanchez, D.J., Aliyari, R., Lu, S., and Cheng, G. (2012). Systematic identification of type I and type II interferon-induced antiviral factors. Proc. Natl. Acad. Sci. U. S. A. *109*, 4239–4244.

96. Liu, W.M., and Zhang, X.A. (2006). KAI1/CD82, a tumor metastasis suppressor. Cancer Lett. *240*, 183–194.

97. Jeong, S.-I., Kim, J.-W., Ko, K.-P., Ryu, B.-K., Lee, M.-G., Kim, H.-J., and Chi, S.-G. (2018). XAF1 forms a positive feedback loop with IRF-1 to drive apoptotic stress response and suppress tumorigenesis. Cell Death Dis. *9*, 806.

98. Yang, R., Sun, L., Li, C.-F., Wang, Y.-H., Yao, J., Li, H., Yan, M., Chang, W.-C., Hsu, J.-M., Cha, J.-H., et al. (2021). Galectin-9 interacts with PD-1 and TIM-3 to regulate T cell death and is a target for cancer immunotherapy. Nat. Commun. *12*, 832.

99. Wu, S.-Y., Fu, T., Jiang, Y.-Z., and Shao, Z.-M. (2020). Natural killer cells in cancer biology and therapy. Mol. Cancer *19*, 120.

100. Brownlie, D., Scharenberg, M., Mold, J.E., Hård, J., Kekäläinen, E., Buggert, M., Nguyen, S., Wilson, J.N., Al-Ameri, M., Ljunggren, H.-G., et al. (2021). Expansions of adaptive-like NK cells with a tissue-resident phenotype in human lung and blood. Proc. Natl. Acad. Sci. U. S. A. *118*. 10.1073/pnas.2016580118.

101. Romee, R., Schneider, S.E., Leong, J.W., Chase, J.M., Keppel, C.R., Sullivan, R.P., Cooper, M.A., and Fehniger, T.A. (2012). Cytokine activation induces human memory-like NK cells. Blood *120*, 4751–4760.

102. Cooper, M.A., Elliott, J.M., Keyel, P.A., Yang, L., Carrero, J.A., and Yokoyama, W.M. (2009). Cytokine-induced memory-like natural killer cells. Proc. Natl. Acad. Sci. U. S. A. *106*, 1915–1919.

103. Gonçalves-Maia, M., Gache, Y., Basante, M., Cosson, E., Salavagione, E., Muller, M., Bernerd, F., Avril, M.F., Schaub, S., Sarasin, A., et al. (2020). NK Cell and Fibroblast-Mediated Regulation of Skin Squamous Cell Carcinoma Invasion by CLEC2A Is Compromised in Xeroderma Pigmentosum. J. Invest. Dermatol. *140*, 1723–1732.

104. Garofalo, C., De Marco, C., and Cristiani, C.M. (2021). NK Cells in the Tumor Microenvironment as New Potential Players Mediating Chemotherapy Effects in Metastatic Melanoma. Front. Oncol. *11*, 754541.

105. Li, H., Handsaker, B., Wysoker, A., Fennell, T., Ruan, J., Homer, N., Marth, G., Abecasis, G., Durbin, R., and 1000 Genome Project Data Processing Subgroup (2009). The Sequence Alignment/Map format and SAMtools. Bioinformatics *25*, 2078–2079.

106. Love, M.I., Huber, W., and Anders, S. (2014). Moderated estimation of fold change and dispersion for RNA-seq data with DESeq2. Genome Biol. *15*, 550.

107. Subramanian, A., Tamayo, P., Mootha, V.K., Mukherjee, S., Ebert, B.L., Gillette, M.A., Paulovich, A., Pomeroy, S.L., Golub, T.R., Lander, E.S., et al. (2005). Gene set enrichment analysis: a knowledge-based approach for interpreting genome-wide expression profiles. Proc. Natl. Acad. Sci. U. S. A. *102*, 15545–15550.

108. Hänzelmann, S., Castelo, R., and Guinney, J. (2013). GSVA: gene set variation analysis for microarray and RNA-seq data. BMC Bioinformatics *14*, 7.

109. Stuart, T., Butler, A., Hoffman, P., Hafemeister, C., Papalexi, E., Mauck, W.M., 3rd, Hao, Y., Stoeckius, M., Smibert, P., and Satija, R. (2019). Comprehensive Integration of Single-Cell Data. Cell *177*, 1888–1902.e21.

110. Shannon, P., Markiel, A., Ozier, O., Baliga, N.S., Wang, J.T., Ramage, D., Amin, N., Schwikowski, B., and Ideker, T. (2003). Cytoscape: a software environment for integrated models of biomolecular interaction networks. Genome Res. *13*, 2498–2504.

111. Langmead, B., and Salzberg, S.L. (2012). Fast gapped-read alignment with Bowtie 2. Nat. Methods *9*, 357–359.

112. Hashimshony, T., Senderovich, N., Avital, G., Klochendler, A., de Leeuw, Y., Anavy, L., Gennert, D., Li, S., Livak, K.J., Rozenblatt-Rosen, O., et al. (2016). CEL-Seq2: sensitive highly-multiplexed single-cell RNA-Seq. Genome Biol. *17*, 77.

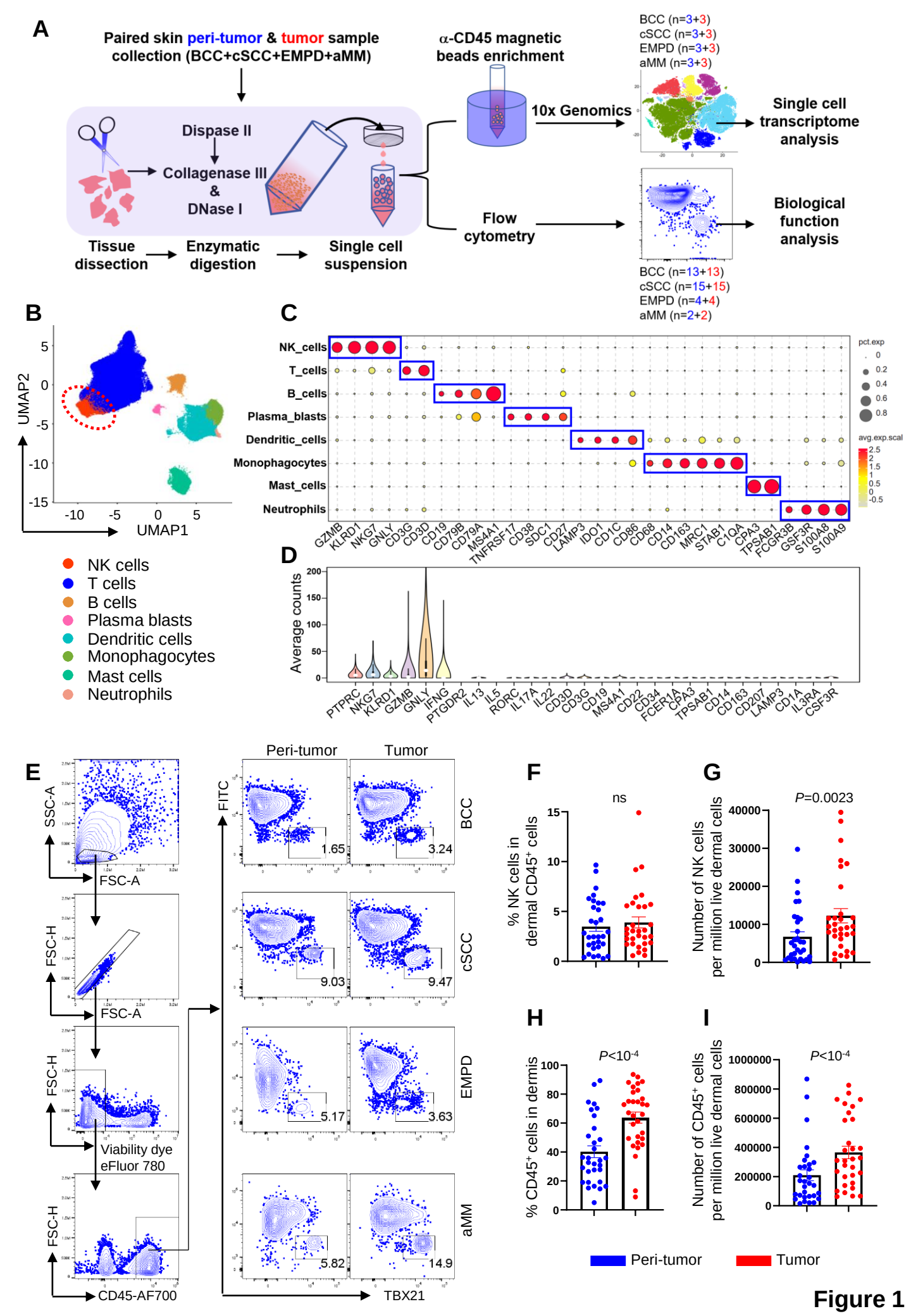
A
Paired skin peri-tumor & tumor sample collection (BCC+cSCC+EMPD+aMM)
Dispase II
Collagenase III & DNase I
Tissue dissection
Enzymatic digestion
Single cell suspension
α-CD45 magnetic beads enrichment
10x Genomics
BCC (n=3+3)
cSCC (n=3+3)
EMPD (n=3+3)
aMM (n=3+3)
Single cell transcriptome analysis
Flow cytometry
BCC (n=13+13)
cSCC (n=15+15)
EMPD (n=4+4)
aMM (n=2+2)
Biological function analysis
B
UMAP2
UMAP1
NK cells
T cells
B cells
Plasma blasts
Dendritic cells
Monophagocytes
Mast cells
Neutrophils
C
NK_cells
T_cells
B_cells
Plasma_blasts
Dendritic_cells
Monophagocytes
Mast_cells
Neutrophils
GZMB KLRD1 NKG7 GNLY CD3G CD3D CD19 CD79B CD79A MS4A1 TNFRSF17 CD38 SDC1 CD27 LAMP3 IDO1 CD1C CD86 CD68 CD14 CD163 MRC1 STAB1 C1QA CPA3 TPSAB1 FCGR3B GSF3R S100A8 S100A9
pct.exp
avg.exp.scal
D
Average counts
PTPRC NKG7 KLRD1 GZMB GNLY IFNG PTGDR2 IL13 IL5 RORC IL17A IL22 CD3D CD3G CD19 MS4A1 CD22 CD34 FCER1A CPA3 TPSAB1 CD14 CD163 CD207 LAMP3 CD1A IL3RA CSF3R
E
SSC-A
FSC-A
FSC-H
Viability dye eFluor 780
CD45-AF700
Peri-tumor
Tumor
FITC
TBX21
BCC
cSCC
EMPD
aMM
1.65
3.24
9.03
9.47
5.17
3.63
5.82
14.9
F
ns
% NK cells in dermal CD45+ cells
G
P=0.0023
Number of NK cells per million live dermal cells
H
P<10-4
% CD45+ cells in dermis
I
P<10-4
Number of CD45+ cells per million live dermal cells
Peri-tumor
Tumor

Figure 1

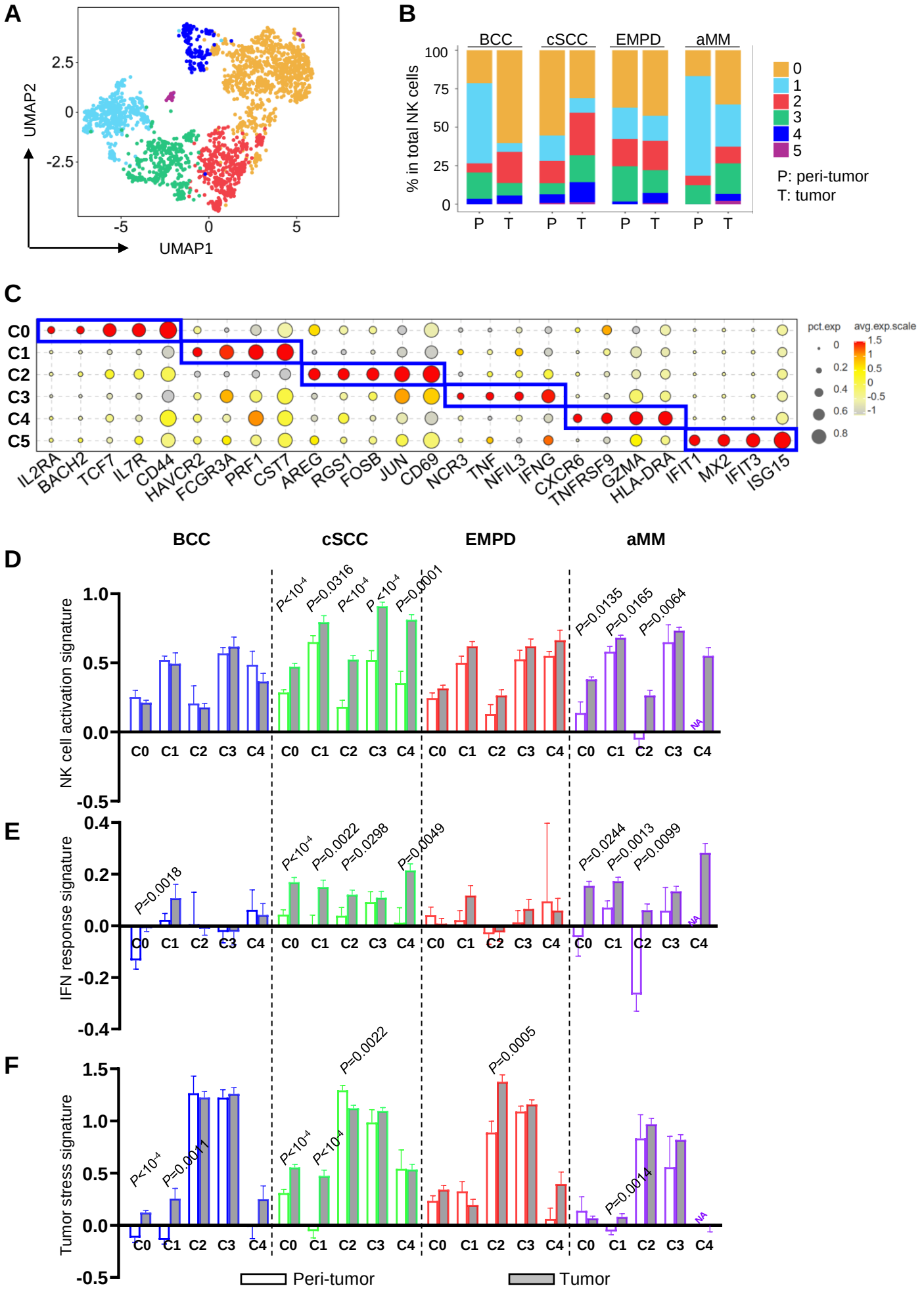
A
UMAP2
UMAP1
2.5
0
-2.5
-5
0
5
B
BCC
cSCC
EMPD
aMM
% in total NK cells
100
75
50
25
0
P
T
0
1
2
3
4
5
P: peri-tumor
T: tumor
C
C0
C1
C2
C3
C4
C5
IL2RA
BACH2
TCF7
IL7R
CD44
HAVCR2
FCGR3A
PRF1
CST7
AREG
RGS1
FOSB
JUN
CD69
NCR3
TNF
NFIL3
IFNG
CXCR6
TNFRSF9
GZMA
HLA-DRA
IFIT1
MX2
IFIT3
ISG15
pct.exp
avg.exp.scale
D
NK cell activation signature
P<10-4
P=0.0316
P<10-4
P<10-4
P=0.0001
P=0.0135
P=0.0165
P=0.0064
NA
E
IFN response signature
P=0.0018
P<10-4
P=0.0022
P=0.0298
P=0.0049
P=0.0244
P=0.0013
P=0.0099
F
Tumor stress signature
P<10-4
P=0.0011
P<10-4
P<10-4
P=0.0022
P=0.0005
P=0.0014
Peri-tumor
Tumor

Figure 2

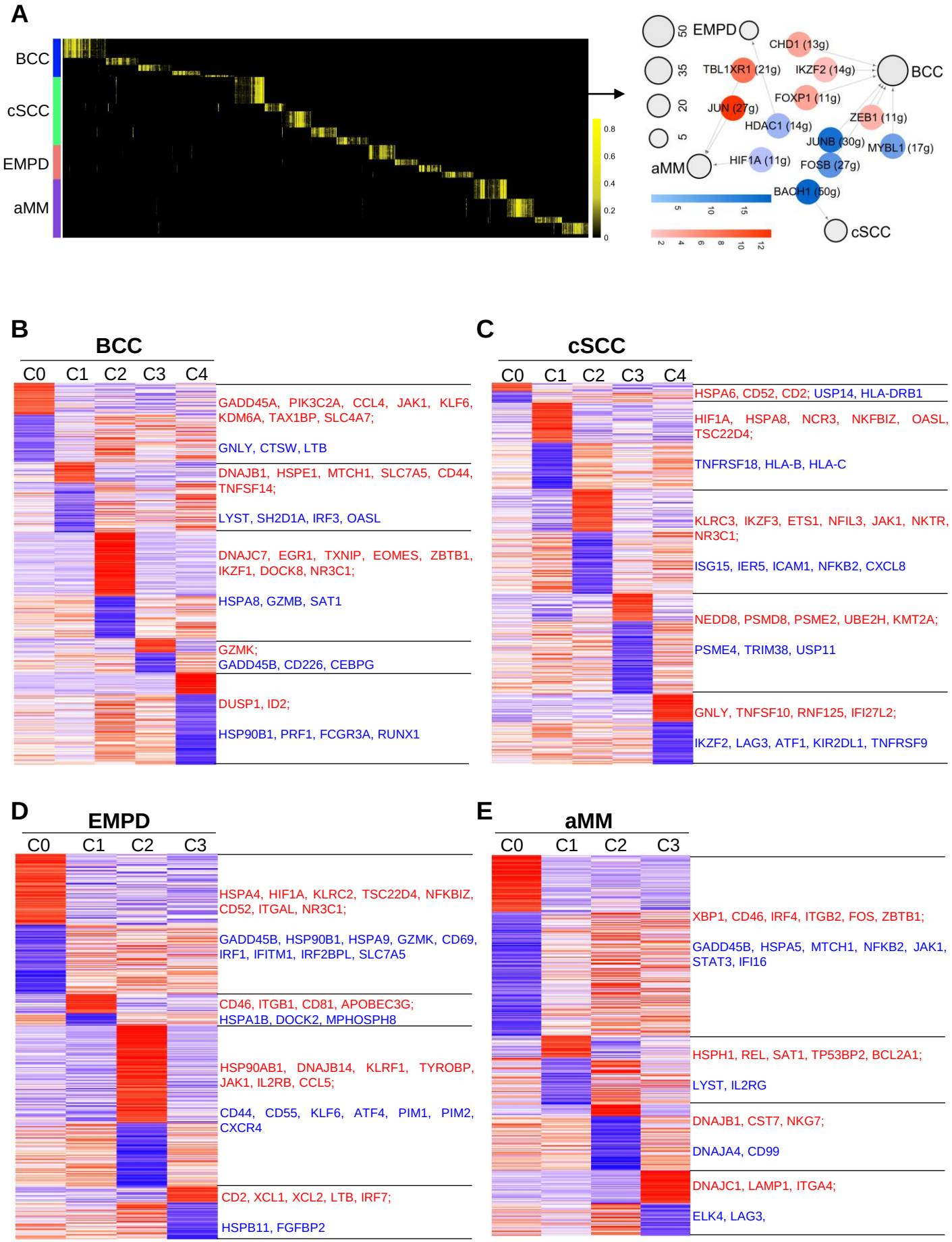
A
BCC
cSCC
EMPD
aMM
0.8
0.6
0.4
0.2
0
EMPD
BCC
aMM
cSCC
50
35
20
5
CHD1 (13g)
TBL1XR1 (21g)
IKZF2 (14g)
FOXP1 (11g)
JUN (27g)
HDAC1 (14g)
ZEB1 (11g)
JUNB (30g)
MYBL1 (17g)
HIF1A (11g)
FOSB (27g)
BACH1 (50g)
5
10
15
2
4
6
8
10
12
B
BCC
C0
C1
C2
C3
C4
GADD45A, PIK3C2A, CCL4, JAK1, KLF6, KDM6A, TAX1BP, SLC4A7;
GNLY, CTSW, LTB
DNAJB1, HSPE1, MTCH1, SLC7A5, CD44, TNFSF14;
LYST, SH2D1A, IRF3, OASL
DNAJC7, EGR1, TXNIP, EOMES, ZBTB1, IKZF1, DOCK8, NR3C1;
HSPA8, GZMB, SAT1
GZMK;
GADD45B, CD226, CEBPG
DUSP1, ID2;
HSP90B1, PRF1, FCGR3A, RUNX1
C
cSCC
C0
C1
C2
C3
C4
HSPA6, CD52, CD2; USP14, HLA-DRB1
HIF1A, HSPA8, NCR3, NKFBIZ, OASL, TSC22D4;
TNFRSF18, HLA-B, HLA-C
KLRC3, IKZF3, ETS1, NFIL3, JAK1, NKTR, NR3C1;
ISG15, IER5, ICAM1, NFKB2, CXCL8
NEDD8, PSMD8, PSME2, UBE2H, KMT2A;
PSME4, TRIM38, USP11
GNLY, TNFSF10, RNF125, IFI27L2;
IKZF2, LAG3, ATF1, KIR2DL1, TNFRSF9
D
EMPD
C0
C1
C2
C3
HSPA4, HIF1A, KLRC2, TSC22D4, NFKBIZ, CD52, ITGAL, NR3C1;
GADD45B, HSP90B1, HSPA9, GZMK, CD69, IRF1, IFITM1, IRF2BPL, SLC7A5
CD46, ITGB1, CD81, APOBEC3G;
HSPA1B, DOCK2, MPHOSPH8
HSP90AB1, DNAJB14, KLRF1, TYROBP, JAK1, IL2RB, CCL5;
CD44, CD55, KLF6, ATF4, PIM1, PIM2, CXCR4
CD2, XCL1, XCL2, LTB, IRF7;
HSPB11, FGFBP2
E
aMM
C0
C1
C2
C3
XBP1, CD46, IRF4, ITGB2, FOS, ZBTB1;
GADD45B, HSPA5, MTCH1, NFKB2, JAK1, STAT3, IFI16
HSPH1, REL, SAT1, TP53BP2, BCL2A1;
LYST, IL2RG
DNAJB1, CST7, NKG7;
DNAJA4, CD99
DNAJC1, LAMP1, ITGA4;
ELK4, LAG3,

Figure 3

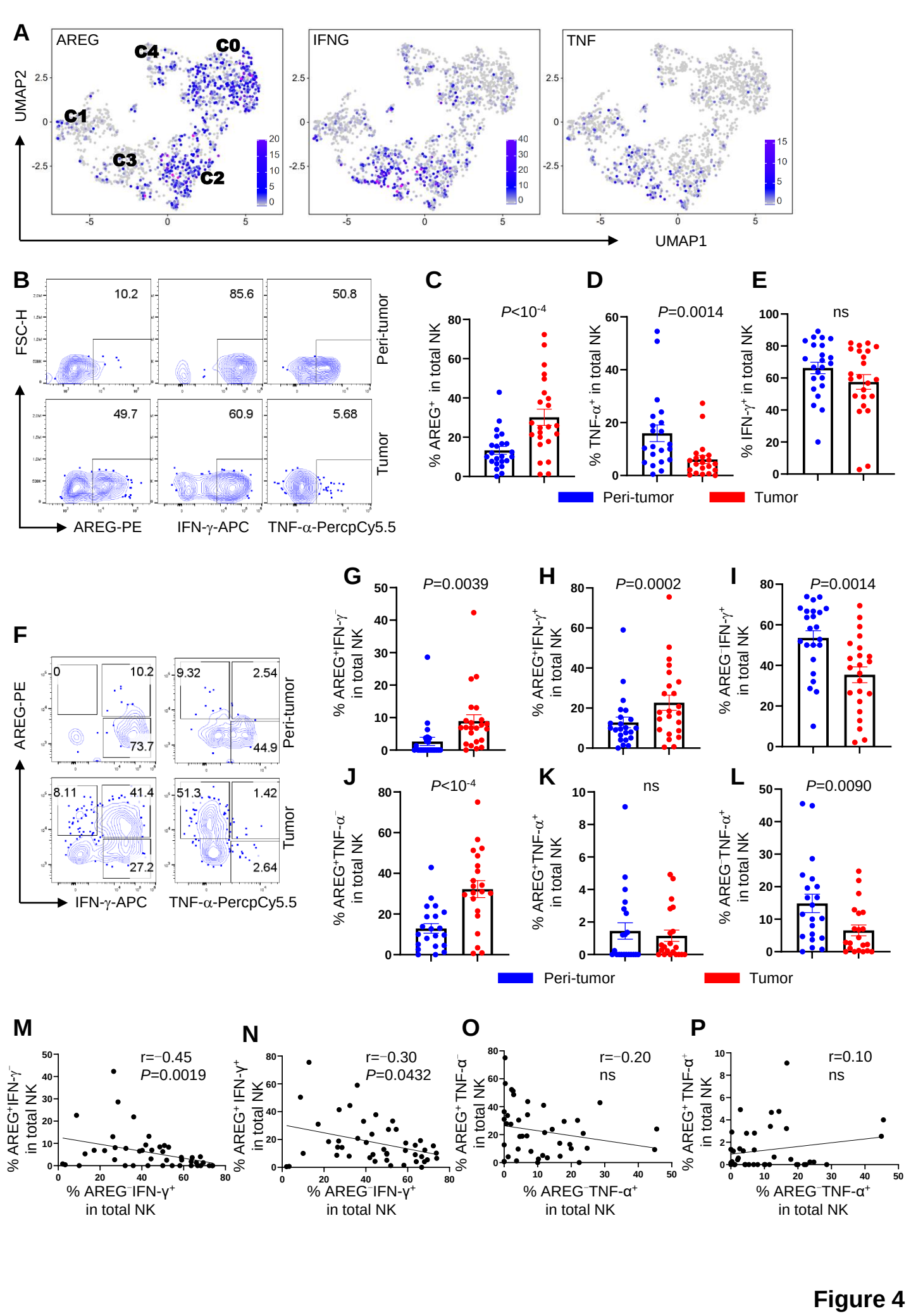
A
AREG
IFNG
TNF
C0
C1
C2
C3
C4
UMAP2
UMAP1
B
FSC-H
10.2
85.6
50.8
49.7
60.9
5.68
Peri-tumor
Tumor
AREG-PE
IFN-γ-APC
TNF-α-PercpCy5.5
C
D
E
P<10-4
P=0.0014
ns
% AREG+ in total NK
% TNF-α+ in total NK
% IFN-γ+ in total NK
Peri-tumor
Tumor
F
AREG-PE
0
10.2
73.7
9.32
2.54
44.9
8.11
41.4
27.2
51.3
1.42
2.64
Peri-tumor
Tumor
IFN-γ-APC
TNF-α-PercpCy5.5
G
H
I
J
K
L
P=0.0039
P=0.0002
P=0.0014
P<10-4
ns
P=0.0090
% AREG+IFN-γ- in total NK
% AREG+IFN-γ+ in total NK
% AREG-IFN-γ+ in total NK
% AREG+TNF-α- in total NK
% AREG+TNF-α+ in total NK
% AREG-TNF-α+ in total NK
Peri-tumor
Tumor
M
N
O
P
r=−0.45
P=0.0019
r=−0.30
P=0.0432
r=−0.20
ns
r=0.10
ns
% AREG+IFN-γ- in total NK
% AREG+ IFN-γ+ in total NK
% AREG+TNF-α- in total NK
% AREG-IFN-γ+ in total NK
% AREG-TNF-α+ in total NK

Figure 4

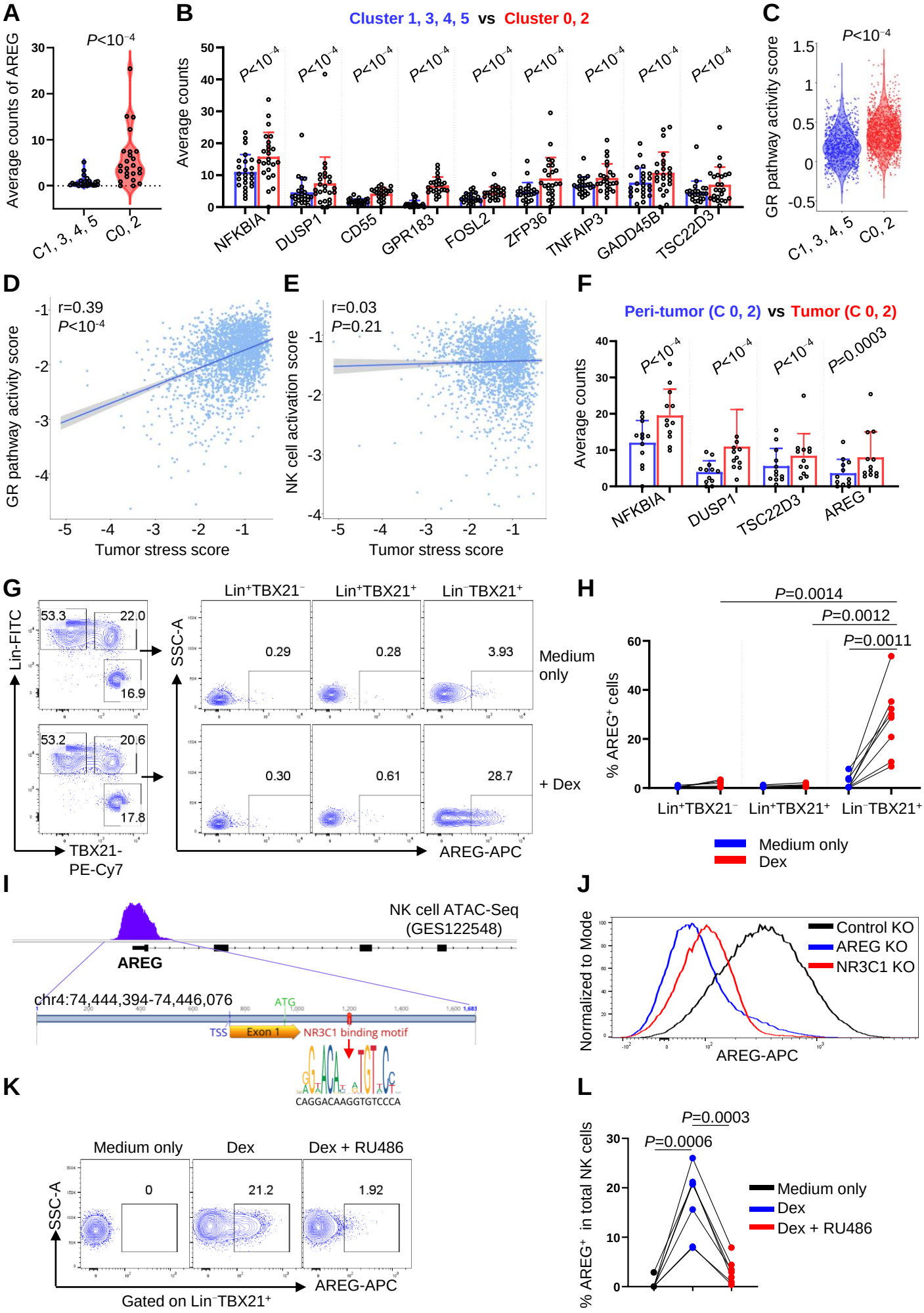
A
Average counts of AREG
P<10⁻⁴
C1, 3, 4, 5
C0, 2
B
Cluster 1, 3, 4, 5 vs Cluster 0, 2
Average counts
NFKBIA
DUSP1
CD55
GPR183
FOSL2
ZFP36
TNFAIP3
GADD45B
TSC22D3
C
GR pathway activity score
D
r=0.39
P<10⁻⁴
GR pathway activity score
Tumor stress score
E
r=0.03
P=0.21
NK cell activation score
Tumor stress score
F
Peri-tumor (C 0, 2) vs Tumor (C 0, 2)
Average counts
P=0.0003
AREG
G
Lin⁺TBX21⁻
Lin⁺TBX21⁺
Lin⁻TBX21⁺
Lin-FITC
SSC-A
TBX21-PE-Cy7
AREG-APC
Medium only
+ Dex
H
P=0.0014
P=0.0012
P=0.0011
% AREG⁺ cells
Medium only
Dex
I
NK cell ATAC-Seq (GES122548)
AREG
chr4:74,444,394-74,446,076
ATG
TSS
Exon 1
NR3C1 binding motif
CAGGACAAGGTGTCCCA
J
Normalized to Mode
Control KO
AREG KO
NR3C1 KO
AREG-APC
K
Medium only
Dex
Dex + RU486
SSC-A
AREG-APC
Gated on Lin⁻TBX21⁺
L
P=0.0003
P=0.0006
% AREG⁺ in total NK cells
Medium only
Dex
Dex + RU486

Figure 5

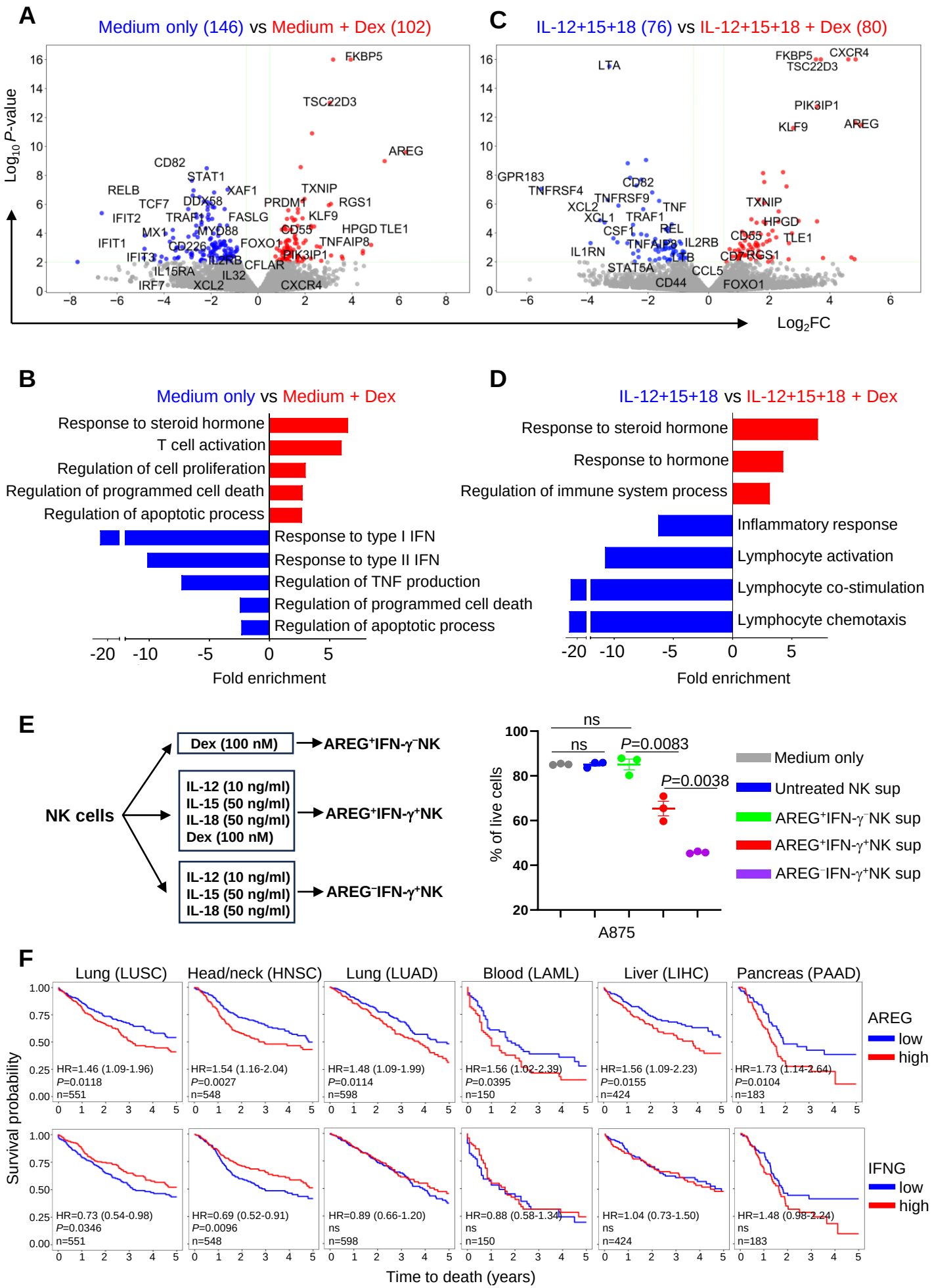
A
Medium only (146) vs Medium + Dex (102)
Log10 P-value
FKBP5
TSC22D3
AREG
CD82
STAT1
RELB
XAF1
TXNIP
TCF7
DDX58
PRDM1
RGS1
IFIT2
TRAF1
FASLG
KLF9
MX1
MYD88
CD55
HPGD
TLE1
IFIT1
CD226
FOXO1
TNFAIP8
IFIT3
IL2RB
PIK3IP1
CFLAR
IL15RA
IL32
IRF7
XCL2
CXCR4
C
IL-12+15+18 (76) vs IL-12+15+18 + Dex (80)
LTA
FKBP5
CXCR4
TSC22D3
PIK3IP1
KLF9
AREG
GPR183
CD82
TNFRSF4
TNFRSF9
XCL2
TNF
TXNIP
XCL1
TRAF1
HPGD
CSF1
REL
CD55
TLE1
TNFAIP8
IL2RB
IL1RN
LTB
CD7
RGS1
STAT5A
CCL5
CD44
FOXO1
Log2FC
B
Medium only vs Medium + Dex
Response to steroid hormone
T cell activation
Regulation of cell proliferation
Regulation of programmed cell death
Regulation of apoptotic process
Response to type I IFN
Response to type II IFN
Regulation of TNF production
Regulation of programmed cell death
Regulation of apoptotic process
Fold enrichment
D
IL-12+15+18 vs IL-12+15+18 + Dex
Response to steroid hormone
Response to hormone
Regulation of immune system process
Inflammatory response
Lymphocyte activation
Lymphocyte co-stimulation
Lymphocyte chemotaxis
Fold enrichment
E
NK cells
Dex (100 nM)
AREG+IFN-γ−NK
IL-12 (10 ng/ml)
IL-15 (50 ng/ml)
IL-18 (50 ng/ml)
Dex (100 nM)
AREG+IFN-γ+NK
IL-12 (10 ng/ml)
IL-15 (50 ng/ml)
IL-18 (50 ng/ml)
AREG−IFN-γ+NK
% of live cells
ns
ns
P=0.0083
P=0.0038
A875
Medium only
Untreated NK sup
AREG+IFN-γ−NK sup
AREG+IFN-γ+NK sup
AREG−IFN-γ+NK sup
F
Lung (LUSC)
Head/neck (HNSC)
Lung (LUAD)
Blood (LAML)
Liver (LIHC)
Pancreas (PAAD)
Survival probability
HR=1.46 (1.09-1.96)
P=0.0118
n=551
HR=1.54 (1.16-2.04)
P=0.0027
n=548
HR=1.48 (1.09-1.99)
P=0.0114
n=598
HR=1.56 (1.02-2.39)
P=0.0395
n=150
HR=1.56 (1.09-2.23)
P=0.0155
n=424
HR=1.73 (1.14-2.64)
P=0.0104
n=183
AREG
low
high
HR=0.73 (0.54-0.98)
P=0.0346
n=551
HR=0.69 (0.52-0.91)
P=0.0096
n=548
HR=0.89 (0.66-1.20)
ns
n=598
HR=0.88 (0.58-1.34)
ns
n=150
HR=1.04 (0.73-1.50)
ns
n=424
HR=1.48 (0.98-2.24)
ns
n=183
IFNG
low
high
Time to death (years)

Figure 6

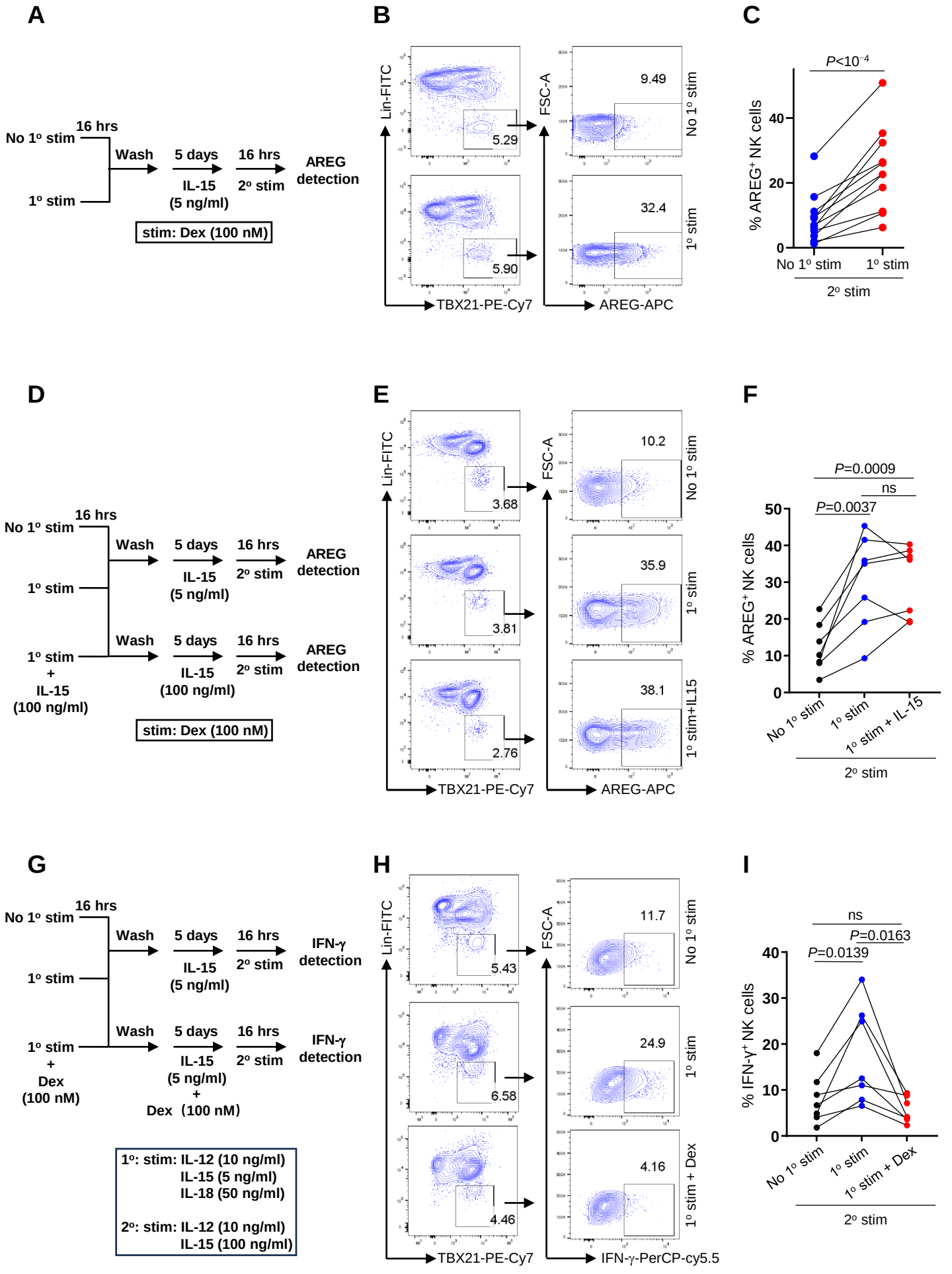
A
No 1º stim
16 hrs
1º stim
Wash
5 days
IL-15
(5 ng/ml)
16 hrs
2º stim
AREG
detection
stim: Dex (100 nM)
B
Lin-FITC
5.29
5.90
TBX21-PE-Cy7
FSC-A
9.49
32.4
AREG-APC
No 1º stim
1º stim
C
P<10⁻⁴
% AREG⁺ NK cells
40
20
0
No 1º stim
1º stim
2º stim
D
No 1º stim
16 hrs
1º stim
Wash
5 days
IL-15
(5 ng/ml)
16 hrs
2º stim
AREG
detection
1º stim
+
IL-15
(100 ng/ml)
Wash
5 days
IL-15
(100 ng/ml)
16 hrs
2º stim
AREG
detection
stim: Dex (100 nM)
E
Lin-FITC
3.68
3.81
2.76
TBX21-PE-Cy7
FSC-A
10.2
35.9
38.1
AREG-APC
No 1º stim
1º stim
1º stim+IL15
F
P=0.0009
ns
P=0.0037
% AREG⁺ NK cells
50
40
30
20
10
0
No 1º stim
1º stim
1º stim + IL-15
2º stim
G
No 1º stim
16 hrs
1º stim
Wash
5 days
IL-15
(5 ng/ml)
16 hrs
2º stim
IFN-γ
detection
1º stim
+
Dex
(100 nM)
Wash
5 days
IL-15
(5 ng/ml)
+
Dex (100 nM)
16 hrs
2º stim
IFN-γ
detection
1º: stim: IL-12 (10 ng/ml)
IL-15 (5 ng/ml)
IL-18 (50 ng/ml)
2º: stim: IL-12 (10 ng/ml)
IL-15 (100 ng/ml)
H
Lin-FITC
5.43
6.58
4.46
TBX21-PE-Cy7
FSC-A
11.7
24.9
4.16
IFN-γ-PerCP-cy5.5
No 1º stim
1º stim
1º stim + Dex
I
ns
P=0.0163
P=0.0139
% IFN-γ⁺ NK cells
40
30
20
10
0
No 1º stim
1º stim
1º stim + Dex
2º stim

Figure 7

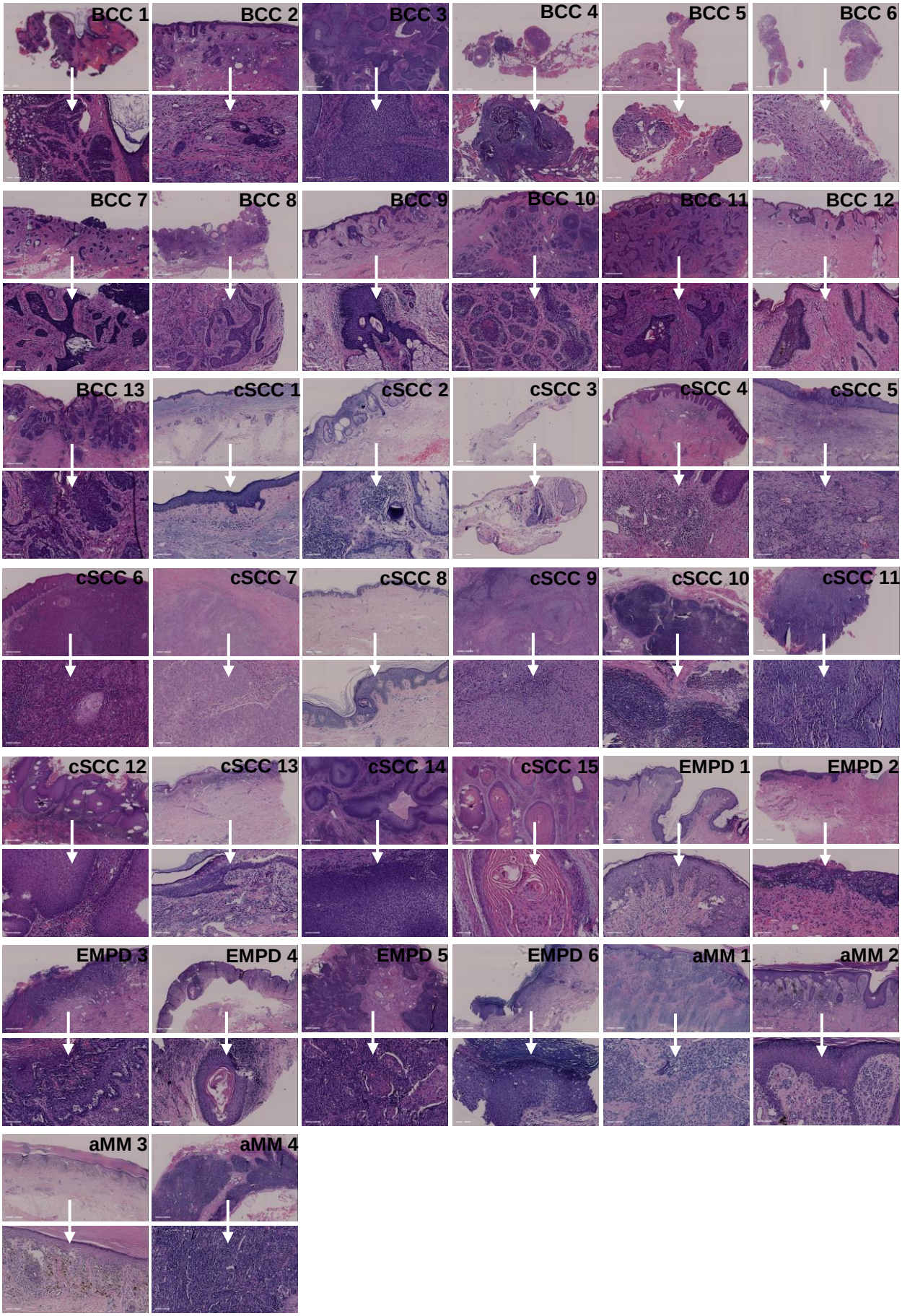
BCC 1
BCC 2
BCC 3
BCC 4
BCC 5
BCC 6
BCC 7
BCC 8
BCC 9
BCC 10
BCC 11
BCC 12
BCC 13
cSCC 1
cSCC 2
cSCC 3
cSCC 4
cSCC 5
cSCC 6
cSCC 7
cSCC 8
cSCC 9
cSCC 10
cSCC 11
cSCC 12
cSCC 13
cSCC 14
cSCC 15
EMPD 1
EMPD 2
EMPD 3
EMPD 4
EMPD 5
EMPD 6
aMM 1
aMM 2
aMM 3
aMM 4

Figure S1

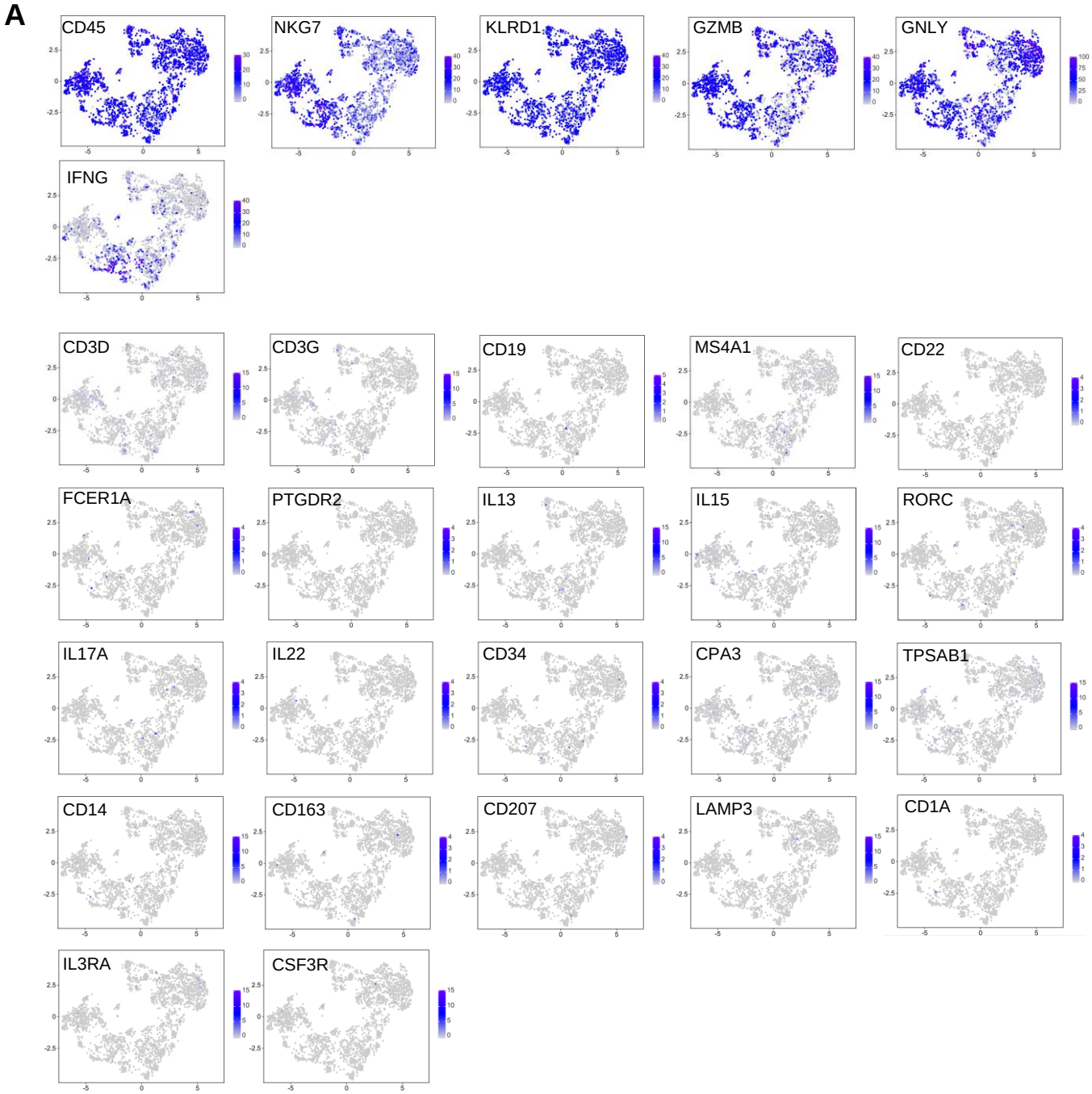
A
CD45
NKG7
KLRD1
GZMB
GNLY
IFNG
CD3D
CD3G
CD19
MS4A1
CD22
FCER1A
PTGDR2
IL13
IL15
RORC
IL17A
IL22
CD34
CPA3
TPSAB1
CD14
CD163
CD207
LAMP3
CD1A
IL3RA
CSF3R

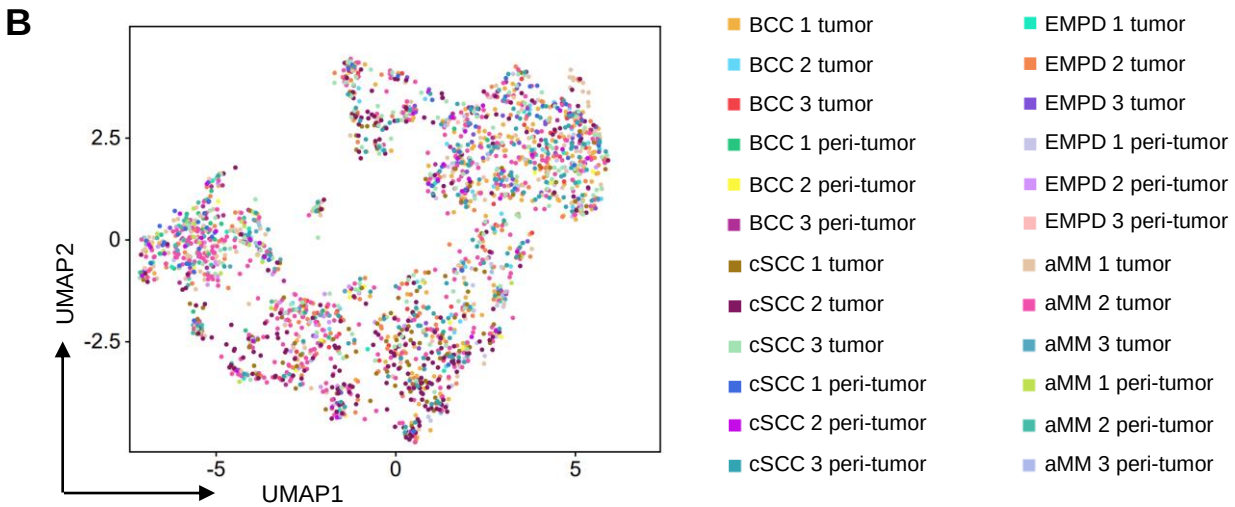
B
UMAP2
UMAP1
2.5
0
-2.5
-5
0
5
BCC 1 tumor
BCC 2 tumor
BCC 3 tumor
BCC 1 peri-tumor
BCC 2 peri-tumor
BCC 3 peri-tumor
cSCC 1 tumor
cSCC 2 tumor
cSCC 3 tumor
cSCC 1 peri-tumor
cSCC 2 peri-tumor
cSCC 3 peri-tumor
EMPD 1 tumor
EMPD 2 tumor
EMPD 3 tumor
EMPD 1 peri-tumor
EMPD 2 peri-tumor
EMPD 3 peri-tumor
aMM 1 tumor
aMM 2 tumor
aMM 3 tumor
aMM 1 peri-tumor
aMM 2 peri-tumor
aMM 3 peri-tumor

Figure S2

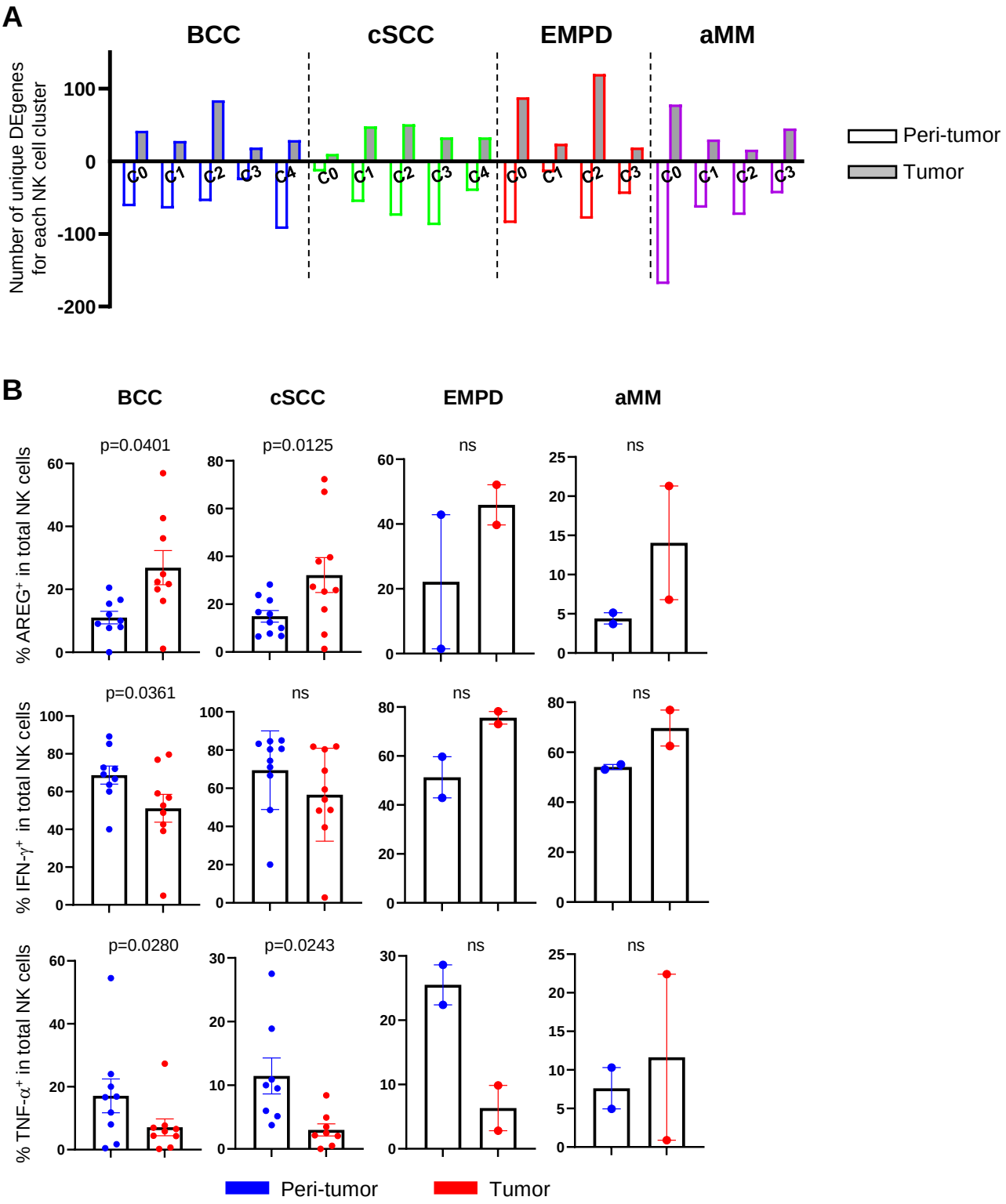
A
BCC
cSCC
EMPD
aMM
Number of unique DEgenes for each NK cell cluster
100
0
-100
-200
C0
C1
C2
C3
C4
Peri-tumor
Tumor
B
BCC
cSCC
EMPD
aMM
% AREG+ in total NK cells
p=0.0401
p=0.0125
ns
ns
% IFN-γ+ in total NK cells
p=0.0361
ns
ns
ns
% TNF-α+ in total NK cells
p=0.0280
p=0.0243
ns
ns
Peri-tumor
Tumor

Figure S3

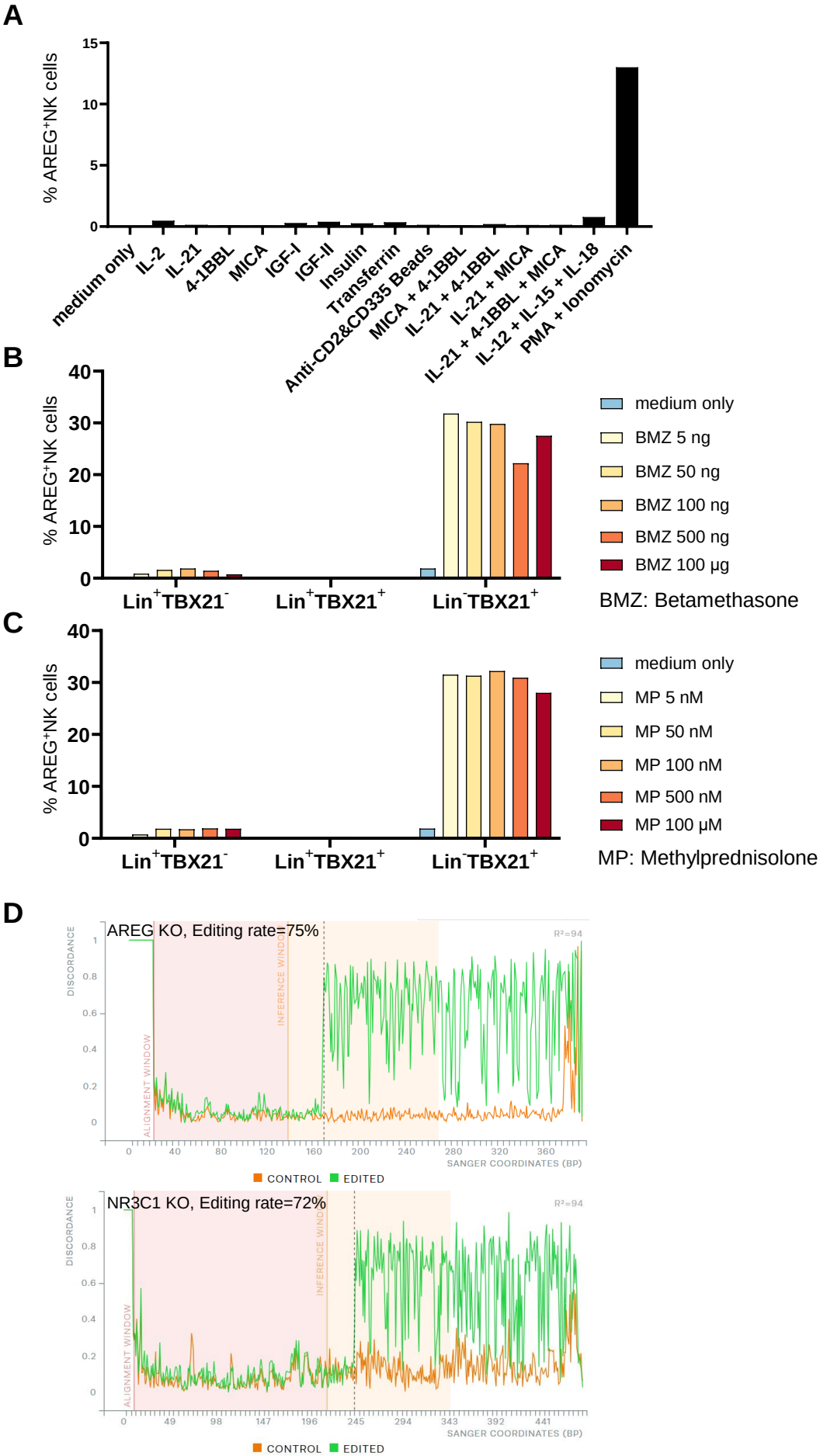
A
% AREG+NK cells
15
10
5
0
medium only
IL-2
IL-21
4-1BBL
MICA
IGF-I
IGF-II
Insulin
Transferrin
Anti-CD2&CD335 Beads
MICA + 4-1BBL
IL-21 + 4-1BBL
IL-21 + MICA
IL-21 + 4-1BBL + MICA
IL-12 + IL-15 + IL-18
PMA + Ionomycin
B
% AREG+NK cells
40
30
20
10
0
Lin+TBX21-
Lin+TBX21+
Lin-TBX21+
medium only
BMZ 5 ng
BMZ 50 ng
BMZ 100 ng
BMZ 500 ng
BMZ 100 µg
BMZ: Betamethasone
C
% AREG+NK cells
40
30
20
10
0
Lin+TBX21-
Lin+TBX21+
Lin-TBX21+
medium only
MP 5 nM
MP 50 nM
MP 100 nM
MP 500 nM
MP 100 µM
MP: Methylprednisolone
D
AREG KO, Editing rate=75%
DISCORDANCE
ALIGNMENT WINDOW
INFERENCE WINDOW
R²=94
SANGER COORDINATES (BP)
CONTROL
EDITED
NR3C1 KO, Editing rate=72%
DISCORDANCE
ALIGNMENT WINDOW
INFERENCE WINDOW
R²=94
SANGER COORDINATES (BP)
CONTROL
EDITED

Figure S4

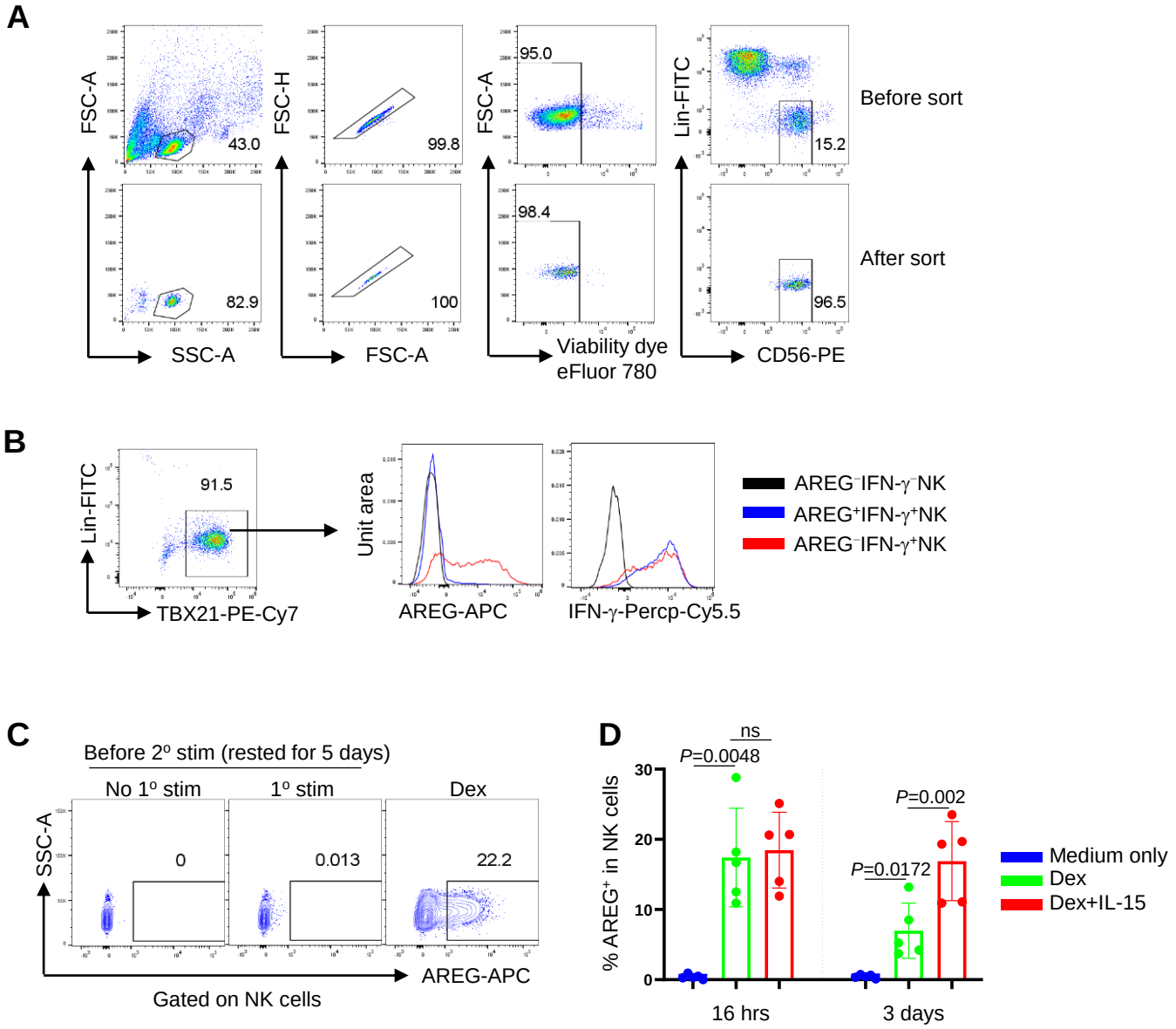
A
FSC-A
SSC-A
43.0
82.9
FSC-H
FSC-A
99.8
100
FSC-A
Viability dye eFluor 780
95.0
98.4
Lin-FITC
CD56-PE
15.2
96.5
Before sort
After sort
B
Lin-FITC
TBX21-PE-Cy7
91.5
Unit area
AREG-APC
IFN-γ-Percp-Cy5.5
AREG⁻IFN-γ⁻NK
AREG⁺IFN-γ⁺NK
AREG⁻IFN-γ⁺NK
C
Before 2º stim (rested for 5 days)
No 1º stim
1º stim
Dex
SSC-A
0
0.013
22.2
AREG-APC
Gated on NK cells
D
% AREG⁺ in NK cells
ns
P=0.0048
P=0.002
P=0.0172
16 hrs
3 days
Medium only
Dex
Dex+IL-15

Figure S5